SYNTHESES OF BENZODITHIOPHENE AND THIENOPYRROLEDIONE CONTAINING CONJUGATED RANDOM POLYMERS AS COMPONENTS FOR ORGANIC SOLAR CELLS

A THESIS SUBMITTED TO
THE GRADUATE SCHOOL OF NATURAL AND APPLIED SCIENCES
OF
MIDDLE EAST TECHNICAL UNIVERSITY

BY

ÖZGE AZERİ

IN PARTIAL FULFILLMENT OF THE REQUIREMENTS
FOR
THE DEGREE OF MASTER OF SCIENCE
IN
CHEMISTRY

MAY 2017

Approval of the thesis:

SYNTHESES OF BENZODITHIOPHENE AND THIENOPYRROLEDIONE CONTAINING CONJUGATED RANDOM POLYMERS AS COMPONENTS FOR ORGANIC SOLAR CELL

submitted by **ÖZGE AZERİ** in partial fulfillment of the requirements for the degree of **Master of Science in Chemistry Department, Middle East Technical University** by,

Prof. Dr. Gülbin Dural Ünver _____
Dean, Graduate School of **Natural and Applied Sciences**

Prof. Dr. Cihangir Tanyeli _____
Head of Department, **Department of Chemistry**

Assoc. Prof. Dr. Ali Çırpan _____
Supervisor, **Department of Chemistry, METU**

Examining Committee Members:

Prof. Dr. Levent Toppare _____
Chemistry Dept., METU

Assoc. Prof. Dr. Ali Çırpan _____
Chemistry Dept., METU

Assoc. Prof. Dr. Dilber Esra Yıldız _____
Physics Dept., Hitit University

Assoc. Prof. Dr. İrem Erel Göktepe _____
Chemistry Dept., METU

Assist. Prof. Dr. Görkem Günbaş _____
Chemistry Dept., METU

Date: 26/05/2017

I hereby declare that all information in this document has been obtained and presented in accordance with academic rules and ethical conduct. I also declare that, as required by these rules and conduct, I have fully cited and referenced all material and results that are not original to this work.

Name, Last name: Özge Azeri

Signature:

ABSTRACT

SYNTHESES OF BENZODITHIOPHENE AND THIENOPYRROLEDIONE CONTAINING CONJUGATED RANDOM POLYMERS AS COMPONENTS FOR ORGANIC SOLAR CELLS

Azeri, Özge

M. S., Department of Chemistry

Supervisor: Assoc.Prof. Dr. Ali Çırpan

May 2017, 65 pages

In recent years organic solar cells (OSC) have attracted considerable attention as promising candidates for renewable energy technology because of their low cost, light weight and flexibility. In this study, in order to improve the efficiency of a bulk heterojunction solar cell, two conjugated random polymers were designed. For this purpose, benzodithiophene and thienopyrroledione containing two random copolymers were synthesized. The effects of several acceptors such as benzotriazole and benzothiadiazole on optoelectronic properties and the performance of bulk heterojunction polymer solar cells were investigated. Electrochemical and optical studies prove that these polymers could be candidates for organic solar cell applications. Both copolymers were n-and p- dopable. Thus, the HOMO and LUMO values were determined by using cyclic voltammetry resulted with the values -5.53 and -3.43 eV for **P1** and -5.54 and -3.53 for **P2**, respectively. The optical band gap of the polymers were calculated by using UV-VIS-NIR spectroscopy as 2.10 and 2.01 eV

for **P1** and **P2**, correspondingly. Bulk-heterojunction solar cells were constructed with the configuration of ITO/PEDOT:PSS/Polymer:$PC_{71}BM$/LiF/Al and the synthesized polymers were used as the electron donors and $PC_{71}BM$ as the electron acceptor in the active layer. The best performance is observed for device of **P2** 1:2 (w:w) ratio with a PCE of 5.83 % under standard AM 1.5 G at 100 mW/cm^2.

Keywords: Benzodithiophene, Thienopyrroledione, Random conjugated polymer, Organic solar cell, Benzothiadiazole

ÖZ

BENZODİTİYOFEN VE TİYENOPİROLDİYON İÇEREN RASTGELE KONJÜGE POLİMERLERİN ORGANİK GÜNEŞ HÜCRELERİ İÇİN SENTEZİ

Azeri, Özge

Yüksek Lisans, Kimya Bölümü

Tez Yöneticisi: Doç.Dr. Ali Çırpan

Mayıs 2017, 65 sayfa

Son yıllarda organik güneş hücreleri düşük maliyetleri, hafif ve esnek olmaları gibi avantajları sebebiyle yenilenebilir enerji teknolojileri alanında umut verici olmaları sebebiyle büyük ilgi görmektedirler. Bu çalışmada organik yığın hetero bağıntılı güneş hücrelerinin verimini arttırmak için rastgele konjüge iki polimer tasarlanmıştır. Bu sebeple benzoditiyofen ve tiyenopiroldiyon içeren rastgele konjuge polimerler sentezlenmiş olup, benzotriazol ve benzothiadiazol akzeptör gruplarının değiştirilmesinin, polimerin optoelektronik özelliklerine ve organik yığın heterobağıntılı polimer güneş hücrelerinin performanslarına etkileri araştırılmıştır. Elektrokimyasal ve optik çalışmaların sonuçları, sentezlenen polimerlerin organik güneş hücreleri uygulamaları için uygun olduğunu göstermiştir. Her iki polimer de n- ve p- katkılanabilirdir. Bu sayede, dönüşümlü voltametri yöntemi kullanılarak polimerlerin HOMO ve LUMO değerleri **P1** için -5.53 ve -3.43 eV , **P2** için -5.54 ve -3.53 eV olarak hesaplanmıştır. UV-Vis-NIR spektrometresi kullanılarak polimerlerin optik bant aralıkları **P1** ve **P2** için sırasıyla 2.10 ve 2.10 eV olarak belirlenmiştir.

ITO/PEDOT:PSS/Polimer:$PC_{71}BM$/LiF/Al konfigurasyonunda yapılan organik güneş hücrelerinin aktif yüzeyinde sentezlenen polimerler elektron verici olarak, PCBM ise elektron alıcı olarak kullanılmıştır. **P2** ve PCBM'nin 1:2 oranında karıştırılarak aktif yüzey olarak kaplandığı organik güneş hücresi standart AM 1.5 G aydınlatması ile en yüksek verimi 5.83% olarak göstermiştir.

Anahtar kelimeler: Benzoditiyofen, tiyenopiroldiyon, rastgele konjüge polimer, organik güneş hücresi, benzothiadiazol

To my precious brother, mother and father

ACKNOWLEDGMENTS

First and foremost, my deepest gratitude goes to my supervisor, Assoc. Prof. Dr. Ali Çırpan; for the opportunity he gave me to work in his research group and for his thoughtful guidance and endless patience throughout my thesis study. Without doubt, his advices will have a big impact in my future life.

I am highly grateful to Prof. Dr. Levent Toppare for his guidance and valuable comments. I have learned a lot from our group meetings.

I would like to express my feelings to Ece Aktaş for her friendship, motivation and support for my thesis study.

I would also thank Dr. Naime Akbaşoğlu Ünlü and Şevki Can Cevher for support and precious guidance.

Special thanks Aslı and Özge, and my past and present laboratory mates Hande, Cansel, Emre, Nima, Janset, Sultan, Duygu, Dr. Fatma Demir and Assoc. Prof. Dr. Ahmet Özgür Saf for their friendships and a peaceful laboratory environment. They made laboratory joyful and I feel lucky being a part of Cirpan Research Group.

I am grateful to Dr. Şerife Özdemir Hacıoğlu and Çağla İstanbulluoğlu for their help in electrochemical and organic solar cell device studies.

I would like to thank my amazing friends, Başak Sezgi Bilen, Zeynep Alatüfek and Zeynep Şule Kenar, Yasemin Durmuş, İpek Önk, Zuhal Selvi Vanlı, Gilda Afshari, Havle Güney and Cansu Bayram for their friendships, encouragements and motivations.

Special thanks Doğuşcan Ahiboz for his understanding, help and love. Life would be much harder without him.

Words cannot express my gratitude to my *little* brother, my lovely mom and dad. Thank you so much for being always by me, endless love and support. And I always feel very lucky and happy to be a part of such a big family. Thank you all my cousins-siblings, uncles and aunts.

The last but not the least, I am very grateful to the beautiful people that I could not share these moments for their valuable contributions to my life and for the unforgettable memories they left behind. I wish we could have more time together.

TABLE OF CONTENT

LIST OF TABLES

LIST OF FIGURES

LIST OF ABBREVATIONS

CP	Conjugated polymer
BHJ	Bulk Heterojunction
OSC	Organic solar cell
EC	Electrochromic
OLED	Organic light emitting diode
OFET	Organic field effect transistor
PCE	Power conversion efficiency
D-A	Donor-Acceptor
HOMO	Highest occupied molecular orbital
LUMO	Lowest unoccupied molecular orbital
CB	Conduction band
VB	Valence band
WO_3	Tungsten trioxide
BLA	Bond length alternation
CV	Cyclic voltammetry
ITO	Indium tin oxide
PSS	Polystyrene sulfonate
PEDOT	Polyethylene dioxythiophene
PCBM	[6,6]-Phenyl C 71 butyric acid methyl ester
$TBAPF_6$	Tetrabutylammonium hexafluorophosphate

ACN	Acetonitrile
η_e	Power conversion efficiency
J_{sc}	Short circuit current density
V_{oc}	Open circuit voltage
FF	Fill factor
P_{max}	Maximum power
P_{in}	Power of the incident light
R_{sh}	Shunt resistor
Rs	Series resistor
AM 1.5 G	Air mass 1.5 global
Eg^{op}	Optical band gap
Eg^{el}	Electronic band gap
TGA	Thermal gravimetry analysis
DSC	Differential scanning calorimetry
UV	Ultraviolet
Vis	Visible
NIR	Near infrared
TPD	Thienopyrroledione
BDT	Benzodithiophene
BTz	Benzotriazole
BT	Benzothiadiazole
PPV	Poly(p-phenylene vinylene)
EQE	External quantum efficiency

CHAPTER 1

INTRODUCTION

1.1. Conjugated Polymers

Polymers are macromolecules that contain repeating units of a large number of reactive small molecules in a sequence. The properties of polymers are determined by their chemical composition, molecular weight, molecular structure and morphology.[1] Polymers were used as insulating materials such as surrounding copper wires until the discovery of conducting polymers. These conducting polymers are called as conjugated polymers owing to the alternating single and double bonds in the main chain.[2] As a result of their discovery and development of conductive polymers, the Nobel Prize in 2000 was given to Alan J. Heeger, Alan G. MacDiarmid and Hideki Shirakawa. After that development, new research areas were created especially in chemistry and physics such as in the field of photochemistry, sensors and energy storage. Besides these, conjugated polymers have been used in Organic Solar Cells (OSCs), Electrochromic Devices (ECDs), Organic Light Emitting Diodes (OLEDs) and Organic Field Effect Transistors (OFETs) due to their rapid switching time, low cost, high optical contrast and ease of proccessibility.[3]

Although the conjugated polymers can conduct electricity, they are not conductive in their neutral state. It is commonly agreed that conducting polymers can be produced via doping process that provides flowing of the electrons as a result of the formation of conduction bands. When a polymer is doped, loosely bounded electrons in conjugated system can able to jump through the polymer chain. By this way, the production of electric current is accomplished. [2]

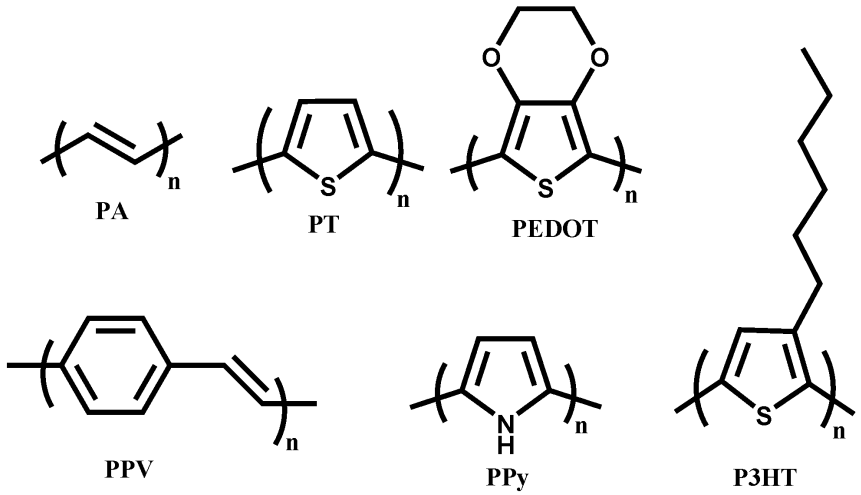

Figure 1. Some Commonly Used Conjugated Polymers

1.1.1. Doping Process

As mentioned in the previous section, conjugated polymers may conduct electricity if they are doped in order to obtain free charges. The band gap of CPs can be adjusted by removing an electron from highest occupied molecular level (HOMO) or by adding an electron to the lowest unoccupied molecular orbital (LUMO). The required charge carriers for providing conductivity can be afforded partial oxidation (p doping) by introducing electron acceptors like AsF_5, I_2 or partial reduction (n doping) by introducing electron donors like K, Na. As a consequence of a doping process, charge defects named as polaron, bipolaron and soliton have been formed.[4,5]

Doping process can be applied in two ways; one of them is chemical doping and the other one is electrochemical doping. Although chemical doping is based on reaction of polymer with a reducing or oxidizing agent, electrochemical doping is carried out by applying voltage to the polymer for an oxidization or reduction.

The process is defined as p type doping in the case of removing of an electron from the polymer backbone. Conversely, during the process of n type doping, introducing of an electron on the polymer chain is resulted in negatively charged anions. After

these, dopants are utilized for the neutralization of these charged particles, which is depicted in scheme.[6]

Chemical Doping of Polyacetylene

$(CH)_n + nyX \longrightarrow [(CH)^{+y} X_y^-]_n$ p-type X = Br_2, I_2

$(CH)_n + nyM \longrightarrow [(CH)^{-y} X_y^+]_n$ n-type M = Na, Li

Electrochemical Doping of Polythiophene

$(T)_n + nyX^- \longrightarrow [T_y^+X_y^-] + nye^-$ p-type X = ClO_4^-

$(T)_n + nyM^+ \longrightarrow [T^+Xy^-]_n$ n-type M = Li^+

While degenerate ground state molecules, similar to polyacetylene form, are designated by solitons, non-degenerate ground state molecules like heterocyclic compounds are known as polarons and bipolarons. Solitons can be positively or negatively charged upon the redox process, which is shown in the Figure 2.

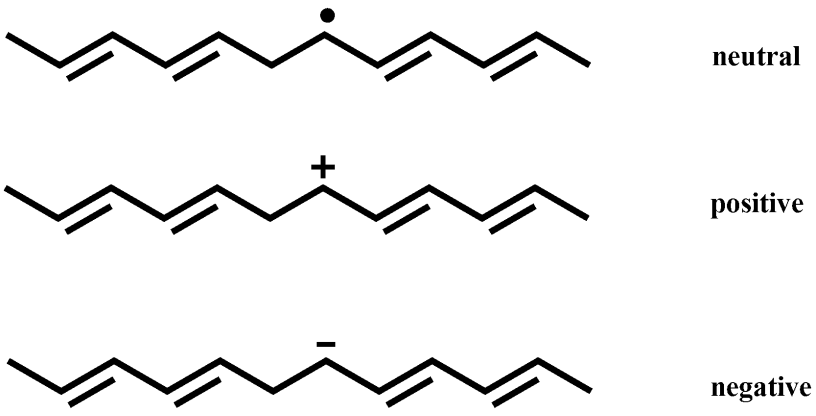

Figure 2. Solitons in trans-polyacetylene

Contrary to degenerate ground state molecules, heterocyclic compounds which have non-degenerate ground state can form radical anions or cations. By ionization of these polymers, polarons are acquired. In addition to polaron, the formation of bipolaron i.e.

dication and dianion structures is available. Figure 3 shows the polaron and bipolaron bands of polypyrrole.[7]

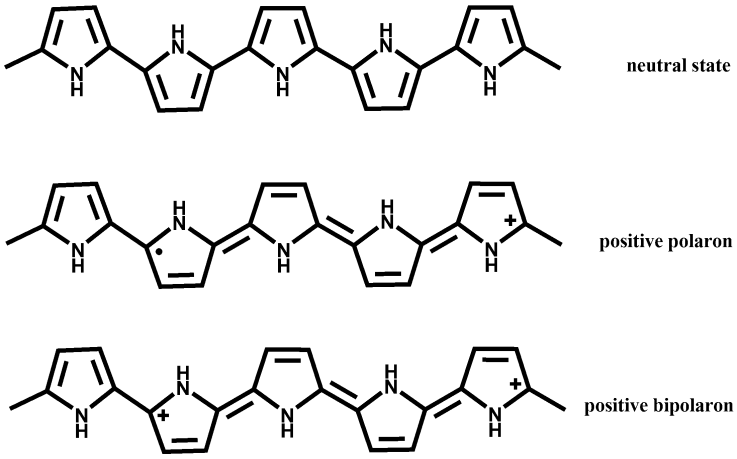

Figure 3. Proposed Structure of Polypyrrole

1.2. Band Gap

The difference between the energy gap between conduction band (CB) and valence band (VB) or highest occupied molecular orbital (HOMO) and lowest unoccupied molecular orbital (LUMO) of a material is known as band gap. The conductivity of a material is related with its band gap. Thus, a material with respect to its electric conductivity may be classified in three main groups as insulators, semiconductors and metals. In Figure 4, a schematic representation of energy band gaps for an insulator, semiconductor and metal is illustrated. The mobility of electrons from HOMO to LUMO induces conductivity.

When the band gap is equal to zero due to the overlapping of VB and CB, this material is defined as a metal. On the contrary, the difference between HOMO and LUMO levels of an insulator is too large and thus the migration of electrons from one band to other is impossible in order to obtain electric conductivity. In between these two type materials, semiconductors take place with smaller band gap than insulators and larger band gap than metals.

The band gap, i.e. energy differences between HOMO and LUMO energy levels, plays a crucial role in optical and optoelectronic properties of conjugated polymers. These properties of a polymer can be adjusted through applying different strategies.[4,8]

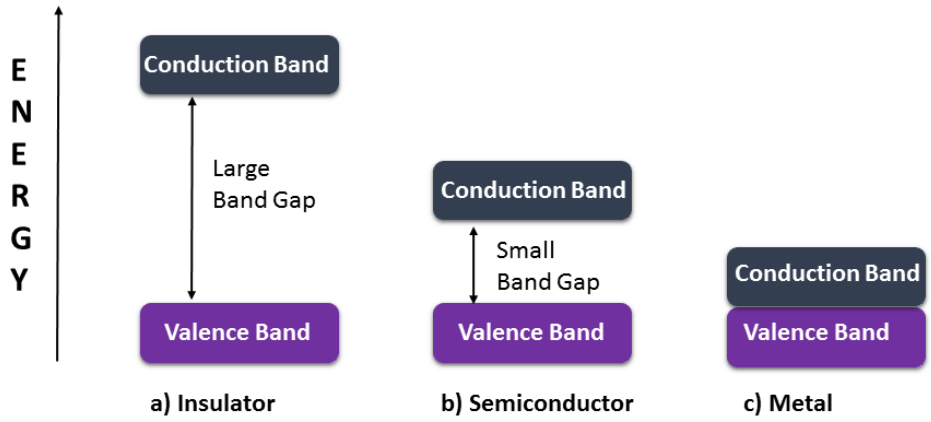

Figure 4. Band Gaps of a) Insulator b) Semiconductor c) Metal

1.2.1. Band Gap Engineering

It is noteworthy to state that tuning of the band gap of conjugated polymers to be used in organic solar cell applications is important since it affects the electronic properties of polymers. This process is called as band gap engineering and is based on some parameters such as intermolecular interactions (E_{Int}), aromaticity (E_{Res}), bond length alternation (E_{BLA}), planarity (E_{θ}) and substituents (E_{Sub}).

The band gap of a polymer is affected by the molecular state of it as polymers can have higher band gap in the solution phase than in the solid state. More rigid and ordered crystalline structure is afforded in the solid state which results in the increasing of intermolecular interactions. Furthermore, this more ordered structure enhances the π-π stacking contributing in red shift on the ground state spectrum and hence lowering in band gap of polymers is obtained.[9]

The band gap of molecules increases when aromaticity in the polymer backbone increases. Since, the π-electron delocalization of electrons on the ring is hindered by aromaticity, it leads to electrons to be less mobile causing in distortion of the conjugation length.[10]

For ground state, there are two possible resonance structures as aromatic and quinoid forms. In aromatic form, each heterocycle retains its aromaticity. On the other hand, the quinoid form is obtained by delocalization of the moving π-electrons along the polymer backbone via converting double bonds into single bonds and at the same time transforming single bonds to double bonds. In this manner, the quinoid form is less stable than the aromatic form and therefore has a smaller band gap. Since, destruction of the aromaticity and a loss in the stabilization energy provide adopting a quinoid structure. The ratio between aromatic and quinoid population in conjugated systems have a correlation with bond length alternation (BLA) defined as the average of the difference in the length between adjacent carbon-carbon bonds. When the aromatic form increases in the ground state, the larger BLA is obtained and also band gap increases. As the quinoid contribution increases, the BLA decreases owing to more double bond character. It is clear to say that BLA depends on the aromatic stabilization resonance energy of the aromatic unit.[11]

Electron delocalization and conjugation is interrupted, if the p orbitals are placed perpendicular rather than overlapping to each other. As conjugation length of a polymer increases, or its planarity decreases, lowering in band gap is observed via decreasing in BLA.[12]

Another effective way to perturbing the molecular orbitals is the incorporation of substituents on the aromatic unit into polymer backbone. In general, electron donating group decreases the energy gap via raising the HOMO energy level, while electron withdrawing groups lower the LUMO energy, and thus band gap is decreased.[13]

1.3. Donor – Acceptor Approach

A common approach for tuning the band gap is to synthesize a conjugated polymer by comprising different type electron rich and electron deficient units to form internal Donor-Acceptor (D-A) structures along the polymer backbone.[14] The bond length alternation, formation of quinoid form and electron delocalization can be controlled by energy band gap of polymers. In 1993, Havinga et al. was discovered this phenomenon for the first time. They claimed that D-A approach lowers the band gap by forming new energy band gap owing to hybridization of the molecular orbital between the donor and acceptor moieties.[11,15] Even though D-A approach arose from the willing of the synthesis of low band gap polymers, this motivation provides control over not only band gap but also energy levels of the conjugated polymers.[16]

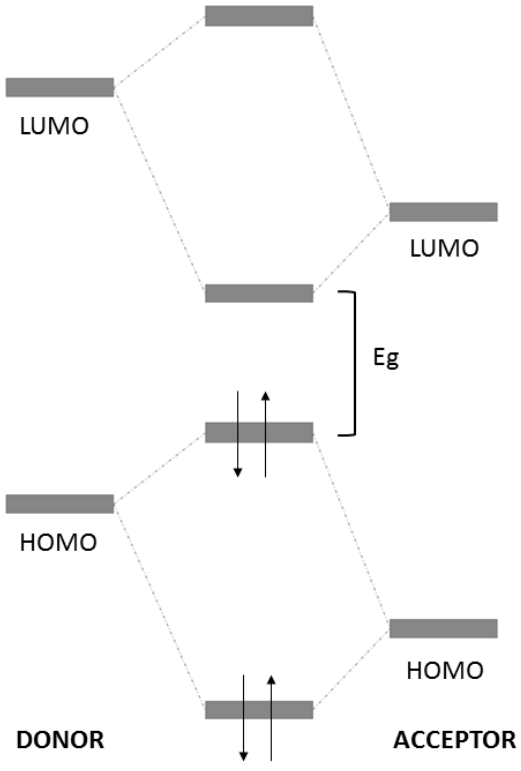

Figure 5. Interaction of the Orbitals in D-A Approach

1.4. Moieties in Donor-Acceptor Approach Conjugated Polymers

1.4.1. Thienopyrroledione Moiety

The thienopyrroledione (TPD) moiety has been accepted as a good acceptor for use in organic solar cells due to their electron-deficient property.[17] Moreover, The TPD moiety has a symmetric, rigidly fused and coplanar structure.[18] These properties can facilitate electron delocalization on the polymer backbone that results with a low band gap and increases the gathering of sunlight.[19] In addition to these, the TPD moiety provides high crystallinity for polymers, high open circuit voltage and highly air stable device through lowering the HOMO of the polymer.[17,20]

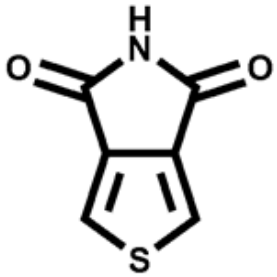

Figure 6. Structure of Thienopyrroledione Moiety

1.4.2. Benzotriazole Moiety

In 2006, Tanimoto and Yamamoto synthesized the first benzotriazole (BTz) containing polymer.[21] This moiety is an n-type electron deficient heterocyclic compound and the properties of BTz can be easily modified by attaching groups on the nitrogen atom.[22] Moreover, the possibility 2-alkylsubstitution of BTz improves the solubility of the synthesized conjugated polymers.[23] Thus, the substitution of the alkyl chain onto benzotriazole unit makes the polymers backbone more planar via preventing steric hindrance. On the other hand, the electron rich nature of benzotriazole moiety causes large band gap owing to high- lying LUMO energy level.[24]

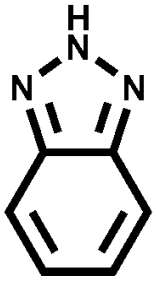

Figure 7. Structure of Benzotriazole Moiety

1.4.3. Benzothiadiazole Moiety

Benzothiadiazole (BT) is one of the most important acceptor moieties due to its ease of preparation, low position of its LUMO energy and good stability. In addition to that, polymers which have BT units reveal suitable properties for optoelectronic applications like low band gaps, high optical contrast, high electric conductivity and broad light absorption in the visible range.[25,26]

Figure 8. Structure of Benzothiadiazole Moiety

1.4.4. Benzodithiophene Moiety

In literature, there are a number of examples with benzodithiophene (BDT) containing polymers and small molecules with more than 10% PCE in organic photovoltaics. [27,28,29] Thus, BDT is a widely used donor moiety for highly efficient organic solar cells

owing to its planarity and symmetrical conjugated structure that may improve ordered π-π stacking in a large domain size. [30, 31]

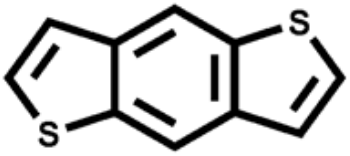

Figure 9. Structure of Benzodithiophene Moiety

1.5. Electrochromism

Electrochromism is defined as the reversible color change in a material by applied external potential.[32,33] When chemical species may be electrochemically switched between different colors, they are said to be electrochromic (EC). In other words, the generation of different visible region electronic absorption bands on shifting between states results in electrochromism. The change in color can be both transparent state to colored one or between two colored states. In cases observed more than two redox states, the material is defined as polyelectrochromic.

Electrochromic species can be sorted as metal oxide films, viologens, and conjugated polymers. WO_3 is the most studied electrochromic metal oxide. Although WO_3 is yellow, WO_2 is brown. During electrochemical reduction process, loss of oxygen generates an additional valence state in the parent WO_3. Secondly, other EC materials like viologens are transparent in the stable dicationic state. For instance, while viologens are transparent in their neutral state or dication form, methyl group substituted viologens are blue in their radical cation form. In addition, n-heptyl substituted viologens have purple color.

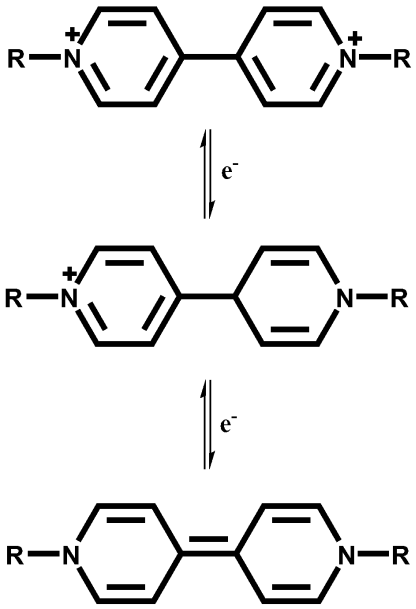

Figure 10. Formation Viologens Radical Cations

The third class of EC materials are conjugated polymers which have gained great interest due to fast response time, high optical contrast, ease of production and modification of their structures. Neutral i.e. undoped form of conjugated polymers are electrically insulators. The doping process enables to introduce polarons and provides major charge carriers on the polymer backbone.[34]

There are some important parameters affecting properties of electrochromic devices such as optical contrast, switching time, stability and optical memory.

1.5.1. Optical Contrast

Optical contrast is described as the percent transmittance change (ΔT%) at a specified wavelength where the highest optical contrast is obtained. Additionally, how optically stable of a material can be investigated by analyzing the transmittance change cycles.

1.5.2. Switching Time

Switching time known as switching speed is as the time required for the coloring or bleaching process of an electrochromic material. This parameter is worthy of attention in the applications of dynamic displays and switchable mirrors and especially depends on film thickness, morphology of the thin film and magnitude of the applied potential.

1.5.3. Stability

Electrochromic stability is related with electrochemical stability since the degradation of the active redox couple leads the loss of electrochromic contrast and therefore the performance of the electrochromic material. Irreversible oxidation or reduction at high potentials and side reactions are the common degradation paths.

1.5.4. Optical Memory

Optical memory which is also known as the open-circuit memory is the time the material keeps its absorption state after removal of an electric field. Contrary to solution based electrochromic materials where the soluble electrochromes diffuse away from the electrodes, the electrochromic memory may be longer in solid state electrochromic devices owing to the adhering of electrochromes onto electrodes.

1.6. Organic Solar Cells

Growing worldwide population and increasing energy consumption stimulate the development of new technologies for harvesting sunlight to convert it to the electricity. Although commonly used photovoltaics are inorganic, in last three decades, significant attention has been given to develop organic solar cell devices due to its advantages like low cost, ease of production, and flexibility. This interest contributed by increasing in power conversion efficiency thanks to new materials and different device structures. The first generation of organic solar cell was constructed as single organic layers which was sandwiched between two metal electrodes having different work functions.[35,36] In 1986, C.W. Tang was reported first time thin film, bilayer organic

solar cell with 1% PCE.[37] However, bilayer devices had some problems like exciton diffusion length and required thickness for light absorption. In 1995, Yu et al. discovered the first organic bulk heterojunction by blending PPV derivative as the donor and a fullerene as an acceptor material.[38] In this way, on the contrary to bilayer devices, the limitation of the charge generation at interface was overcome via obtaining donor-acceptor matrix as an active layer.[39]

1.6.1. Device Construction of Bulk Heterojunction OSCs

A bulk heterojunction organic solar cell device is schematically depicted in Figure 11. Generally, a bulk heterojunction organic solar cell device is constructed by coating different layers of specific functional materials. Firstly, a glass substrate is coated with indium-tin oxide (ITO) as the anode. This transparent anode material with a high work function collects holes. After that, in order to smoothen the ITO coated surface, PEDOT:PSS is coated via using spin- coating technique. The layer of PEDOT:PSS helps to facilitate the removing of holes and decreases the work function of ITO.[40] Onto these two layers, active layer is deposited via spin coating. Active layer contains a mixture of synthesized conjugated polymer as donor and fullerene derivatives as acceptor. A blend containing donor-acceptor moieties reduces the distance of exciton travelling owing to its large interface between polymer and fullerene. As a final step, lithium fluoride (LiF) and aluminum (Al) are vacuum-deposited on the top of the active layer in order to form cathode which collects the generated charge carriers. [41,42]

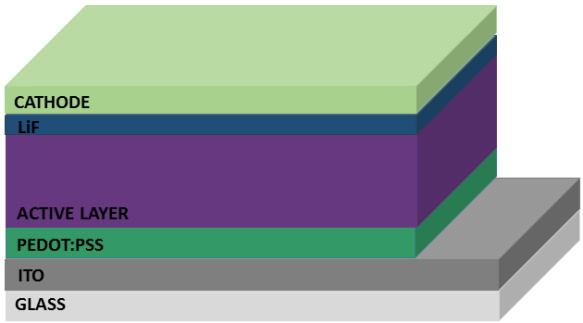

Figure 11. Device Construction of Bulk Heterojunction OSCs

1.6.2. Operation Principle of Organic Solar Cells

The basic working principle of an organic solar cell is illustrated in Figure 12. Firstly, when light comes to the active layer of a device, absorption of light occurs. In this way, an electron in donor moiety is excited from the highest occupied molecular orbital (HOMO) to the lowest unoccupied molecular orbital (LUMO). So, a Frenkel exciton defined as coulombically bound electron-hole pair is formed. In organic materials, binding energy of an exciton is in between 0.5 – 1 eV.

Secondly, after excitons are generated, they diffuse towards donor-acceptor interfaces just before recombining to the ground state. After that, the dissociation into free charges at donor-acceptor interface occurs. Since the diffusion length of an exciton in an organic material is around 5-20 nm. Therefore, the domain size of donor or acceptor is limited to 20 nm that is also a restriction for thickness of the active layer.

The next step is the movement of free charges to the respective electrodes with different work functions and so the circuit is completed. The obtained photocurrent depends on the recombination of the charges during the journey to the electrodes. In addition, interaction between atoms or other charges may limit the obtained current. In order to overcome this problem, charges should overcome the potential barrier of interface. [20,43–48]

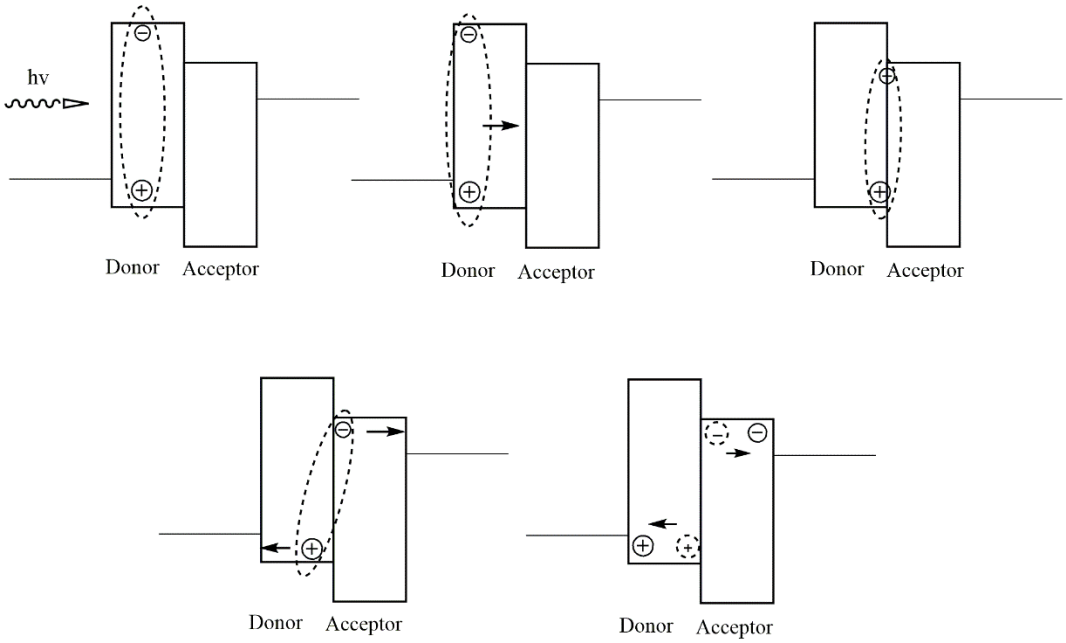

Figure 12. Illustration of Operation Principle of OSCs

1.6.3. Characterization of an Organic Solar Cell Device

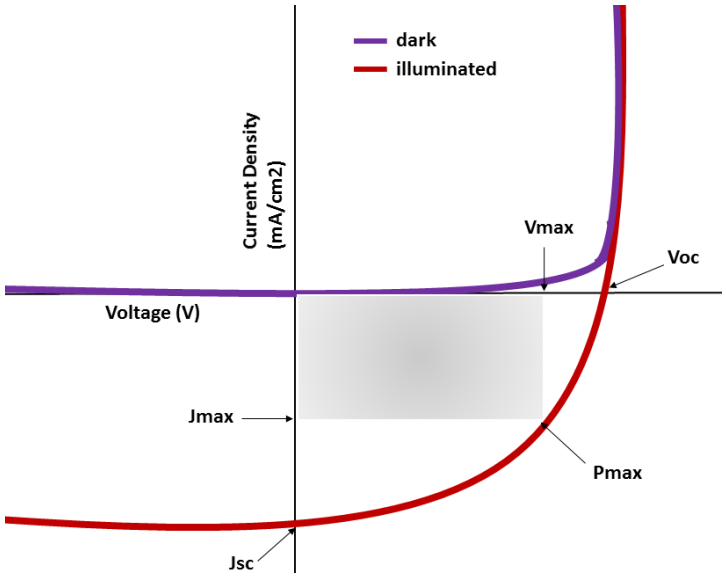

Figure 13. Current Density-Voltage Graph

The current density-voltage (J-V) characteristics in the dark and under illumination are considered to study the performance of an organic solar cell. According to Figure 13, a typical J-V curve of an organic solar cell device has two conditions i.e. under dark and illumination. Without any illumination, the J-V curve passes through the origin because of existing almost no potential. On the other hand, when the device is illuminated, the J-V curve is shifted in the fourth quadrant by the amount of photocurrent generated. The power conversion efficiency (PCE) η_e of an organic solar cell is the ratio between the maximum output power P_{max} and the power of the incident light P_{in}, which is calculated by Eq.1 :

$$\eta e = \frac{Pmax}{Pin} \qquad FF = \frac{Jmax*Vmax}{Jsc*Voc} \qquad Pmax = Voc * Jsc * FF \qquad \textbf{Eq.1}$$

Where V_{oc} is open circuit voltage, J_{sc} is short circuit current, and FF is the fill factor. All measurements are done under AM 1.5 G (Air Mass 1.5 Global) which is described in Figure 14. Air mass (AM) is a measure of how much atmosphere sunlight should travel through to reach the earth's surface. The notation of AM is as AM(x) where x can be defined as the inverse of cosine of the zenith angle of the sun. A standard of AM 1.5 defines that the sun is at an angle of around 48°. AM is not the light intensity, it is, on the contrary, the spectrum of radiation. In order to measure solar cell performances, the intensity is set as 100 mW/cm. [49,50]

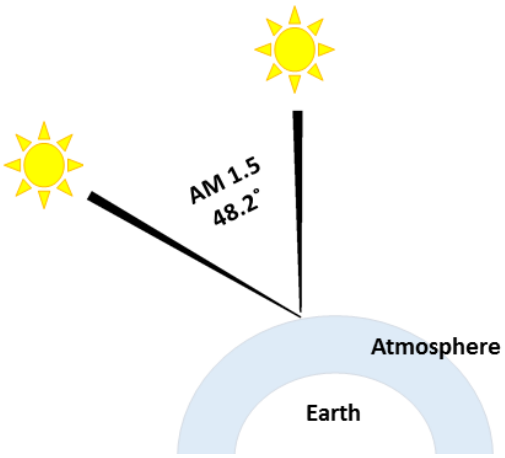

Figure 14. Air Mass 1.5 Global Standardization

1.6.4. Important Parameters for OSC Efficiency

1.6.4.1. Open-Circuit Voltage (Voc)

The open-circuit voltage (V_{oc}) can be defined as the potential difference which is formed between two electrodes. It is already reported that V_{oc} in organic solar cells has a linear relationship between the highest occupied molecular orbital (HOMO) level of the donor and the lowest unoccupied molecular orbital (LUMO) level of the acceptor.[51] Moreover, open-circuit voltage does not depend on electrodes' work functions.[39] In 2006, Scharber et al. proposed an Eq.2 to express V_{oc} after blending many different donor materials with a common acceptor.[52]

$$Voc = \left(\frac{1}{q}\right)\left[E(HOMO)_{donor} - E(LUMO)_{acceptor}\right] - 0.3\,V \qquad \textbf{Eq.2}$$

where q is the elementary charge and 0.3 V is the deviation between the theoretical maximum built-in potential(V_{BI}) and open-circuit voltage.

1.6.4.2. Short-Circuit Current (Jsc)

Short-circuit current is the current which flows through a solar cell when there is no external resistance under illumination. This current is the maximum current produced via a device. [44] The ratio between the number of photons incident on a solar cell device and the number of generated charge carriers gives the external quantum efficiency (EQE) and EQE is related with $J_{sc.}$ Hence, EQE parameters given in Eq.3 affect J_{sc} directly.

$$EQE = \eta abs * \eta diff * \eta diss * \eta tr * \eta cc \qquad \textbf{Eq.3}$$

η_{abs} ; the light absorption yield of the device.

η_{diff} ; the capability of an exciton in order to diffuse to donor-acceptor interface.

η_{diss} ; the dissociation efficiency of excitons.

η_{tr} ; the charge transfer efficiency throughout the device.

η_{cc} ; the efficiency which is related with the ability of collection of charges at corresponding electrodes. [53]

1.6.4.3. Fill Factor (FF)

The power conversion efficiency of a solar device is mainly determined by its fill factor (FF). It basically describes how square the J-V curve is and Eq.4 shows it:

$$Fill\ Factor = \frac{Jmax * Vmax}{Jsc * Voc} \qquad \textbf{Eq.4}$$

where Jmax : the maximum power point current density

Vmax: the maximum power point current voltage

As a result of the recombination of charges at junction points, deviation from the ideal diode is observed and thus, the shape of the J-V curve changes. This can be characterized by the parasitic loss mechanisms of shunt and series resistance. In the case of ideal diode behavior, shunt resistance (R_{sh}) should be infinite. When R_{sh} reduces, imperfections within the active layer of the device or current leaks at the junction point between layers and device bring about the reduction in shunt resistance. On the other hand, series resistance should equal to zero, yet poor conductivity throughout active layer of the device increases shunt resistance.[53]

1.7. Benzodithiophene and Thienopyrroledione Containing Conjugated Polymers for Organic Solar Cells

The concept of D-A approach is one of the most efficient strategies in order to harvest more photon via lowering optical band gap. Recent studies show that D-A type polymers are promising candidates for photovoltaic applications. For example, electron donating materials derived from BDT unit have demonstrated high power

conversion efficiencies when they coupled with electron deficient units like TPD, BTz, BT, diketopyrrolopyrrole (DPP), thienothiophene (TT). [30,54–56]

Since BDT was first utilized as the donor unit in the synthesis of conjugated polymers for organic photovoltaics in 2008, the device performance of BDT containing polymer based solar cells has been an advanced improvement.[57] The first time, in 2010, Zou et al. introduced TPD moiety in a polymer backbone which contains BDT as the donor moiety for photovoltaic devices. They reported the electrochemical band gap as 1.81 eV and the photovoltaic device demonstrated PCE 5.5 % with a Voc of 0.85 V, a Jsc of 9.81 mA/cm^2, and a FF of 0.66 %.[54] In addition, Zhang et al. synthesized a conjugated polymer containing TPD and BDT with a PCE of 4.1 %.[29] In 2012, B.R. Aich et al. investigated TPD and BDT containing polymer via blending with $PC_{60}BM$ and adding additives as 1-chloronapthalene (CN) and 1,8-diiodooctane (DIO), and thus a PCE of 7.1 % was obtained with a Jsc of 10.89 mA/cm^2, a Voc of 0.93 V and a FF of 70 %.[58] Furthermore, in 2015, Liu et al. coupled with TPD with BDT and benzodifuran (BDF), a derivative of BDT. PCE of 2.32 % and 2.04 % were recorded for polymers containing TPD acceptor unit and BDF and BDT donor units, respectively.[59]

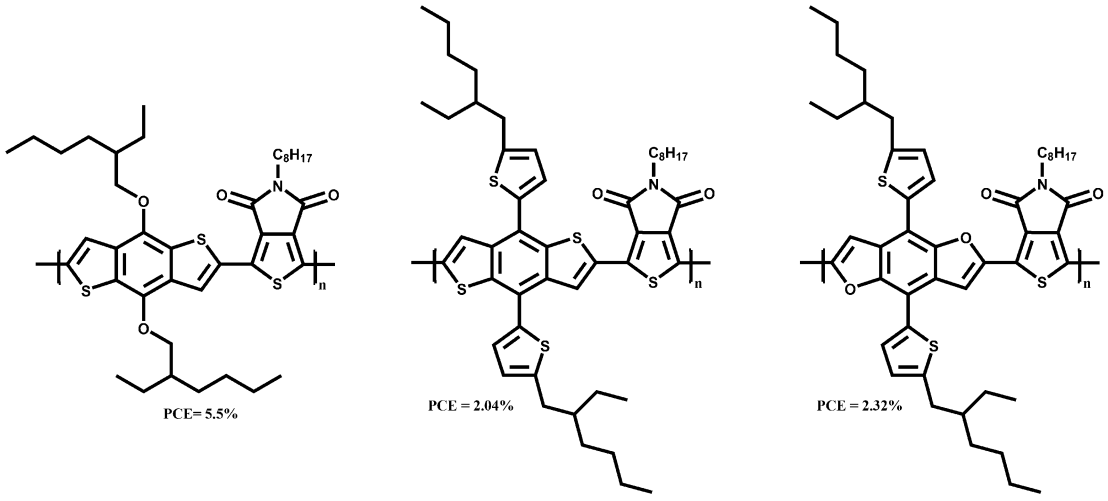

Figure 15. Literature Examples of the Structures and Photovoltaic Performance of BDT and TPD Based Conjugated Polymers

1.8. Aim of the Study

The purpose of the study is to synthesize newly designed random conjugated polymers for organic solar cell applications. Both polymers had one donor and two acceptor moiety and synthesized via Stille coupling reaction. After syntheses of the polymers, their electrochemical and device characterizations were investigated. Benzodithiophene moiety was chosen as the donor and thienopyrroledione, benzotriazole and benzothiadiazole were chosen as the acceptors. The effects of benzotriazole and benzothiadiazole moieties on characteristics of polymers were investigated. Hence, **P1** had benzotriazole moiety while **P2** had benzothiadiazole moiety in polymer backbone. The molecular structures of synthesized polymers were demonstrated in Figure 16. The reason why these moieties were chosen was explained in previous sections.

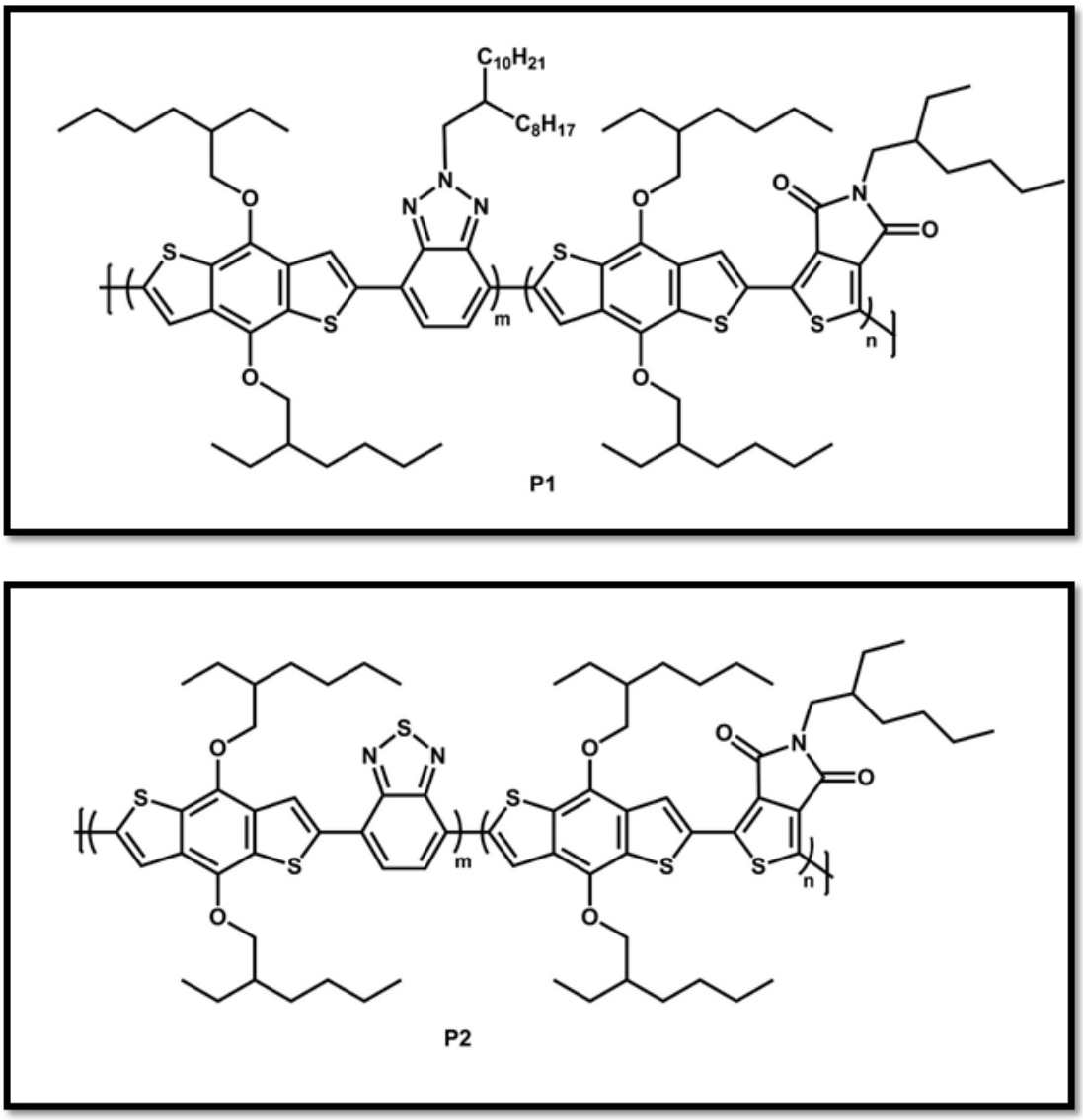

Figure 16. The Molecular Structures of Synthesized Polymers **P1** and **P2**

CHAPTER 2

2. EXPERIMENTAL

2.1. Materials and Equipments

The chemicals for monomers and polymers were purchased from Sigma-Aldrich Chemical Co. Ltd. $PC_{71}BM$ was purchased from Solenne and was used as acceptor moiety in the device. Toluene was dried via metallic sodium and benzophenone and freshly used in the reactions. Other solvents were used without any further processes. Moisture and air sensitive reactions were accomplished under argon atmosphere

In the column chromatography, Merck Silica Gel 60 was used as the stationary phase with different corresponding mobile phase solvents for the purification of the moieties. In order to prove the chemical structures of the monomers and polymers, ^{1}H and ^{13}C NMR spectra of them investigated via using deuterated chloroform ($CDCl_3$) as a solvent. A Bruker Spectrospin Avance DPX-400 Spectrometer was the device with respect to trimethylsilane (TMS) the internal reference. According to the TMS reference, the chemical shifts were stated at 7.26 ppm for ^{1}H and 77 ppm for ^{13}C NMR in the presence of $CDCl_3$ solvent.

2.2. Synthesis of Monomers

2.2.1. Synthesis of 9-(bromomethyl)nonadecane

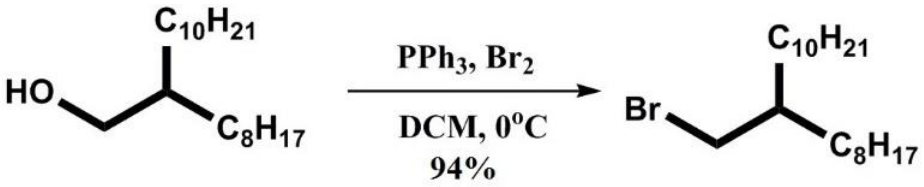

Figure 17. Synthesis of 9-(Bromomethyl)nonadecane

A solution of 2-octyl-1-dodecanol (1.40 g, 4.69 mmol) and triphenylphosphine (PPh_3) (1.25 g, 4.77 mmol) in CH_2Cl_2 (DCM) (20 mL) was cooled to 0˚C in an ice bath. Bromine (0.3 mL, 13.3 mmol) was added drop wise to the reaction mixture and the reaction was stirred for overnight at room temperature. Then, reaction was washed with saturated $NaHSO_3$ solution. Organic layer was further washed with distilled water and brine repeatedly. $MgSO_4$ was used as a drying agent and the solvent was evaporated under reduced pressure. The product was obtained as a colorless oil, after the purification by column chromatography on silica gel using hexane (1.59 g, 94%).

^{1}H NMR (400 MHz, $CDCl_3$), d (ppm): 3.37(d, J= 4.7 Hz, 2H), 1.52 (m, 1.48–1.55, 1H), 1.20 (m, 1.26–1.14, 32 H), 0.80 (t, J =6.8 Hz, 6H).^{13}C NMR (400 MHz, $CDCl_3$), d (ppm): 39.6, 39.5, 32.59, 31.9, 29.8, 29.7, 29.6, 29.5, 29.4, 29.3, 26.6, 22.7, 14.1.

2.2.2. Synthesis of 4,7-dibromobenzo[c][1,2,5]thiadiazole

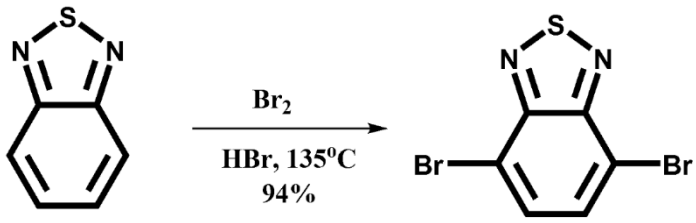

Figure 18. Synthesis of 4,7-Dibromobenzo[c][1,2,5]thiadiazole

A solution of 2,1,3-benzothiadiazole (5.00 g, 36.70 mmol) in 50 mL HBr (47%) was added in a three necked round bottom reaction flask. After 1 hour reflux at 100˚C, a solution of bromine (5.50 mL, 108.27 mmol) in 20 mL HBr (47%) was added into the reaction flask slowly. The reaction mixture was refluxed overnight. The residue was poured into 600 mL concentrated $NaHSO_3$ solution to remove excess Br_2. Then, the obtained solution was filtered to obtained orange solid residue. The obtained solid was washed with distilled water several times and then with cold diethyl ether to afford 4,7-dibromobenzo[c][1,2,5]thiadiazole (10.21 g, yield 94%) as a light-yellow solid.

^{1}H NMR (400 MHz, $CDCl_3$) δ 7.68 (s, 2H). ^{13}C NMR (101 MHz, $CDCl_3$), d (ppm) δ 152.94, 132.36, 113.91.

2.2.3. Synthesis of 3,6-dibromobenzene-1,2-diamine

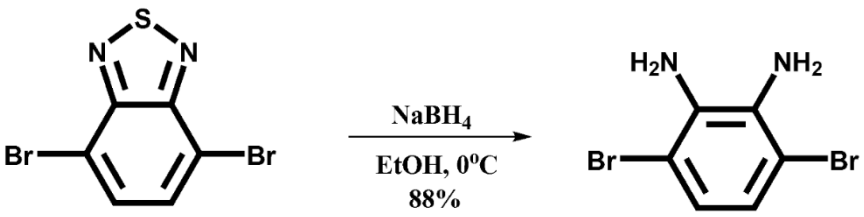

Figure 19. Synthesis of 3,6-Dibromobenzene-1,2-diamine

4,7-Dibromobenzo[c][1,2,5]thiadiazole (10.0 g, 34.0 mmol) was taken into 2000 mL round bottom flask and then 300mL ethanol (EtOH) were added to dissolve it. The system was placed in an ice bath before the addition of the $NaBH_4$ (25.7 g, 680 mmol). After the temperature of the reaction medium was adjusted to the 0˚C, $NaBH_4$ was added portion by portion. After the addition was completed, the system was stirred for overnight at room temperature. The solvent was evaporated and the residual dark solid was dissolved in diethyl ether and washed with four times distilled water. Organic phase was dried over $MgSO_4$ and the solvent was evaporated to obtain the product as a light yellow solid. (8.0 g, yield 88%).

^{1}H NMR (400 MHz, $CDCl_3$) δ 6.85 (s, 2H), 3.91 (s, 4H). ^{13}C NMR (101 MHz, $CDCl_3$) δ 133.74, 123.26, 109.69.

2.2.4. Synthesis of 4,7-dibromo-2H-benzo[d][1,2,3]triazole

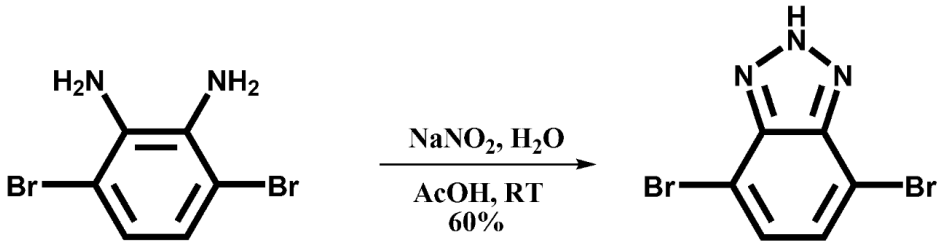

Figure 20. Synthesis of 4,7-Dibromo-2H-benzo[d][1,2,3]triazole

3,6-Dibromobenzene-1,2-diamine (5.00 g, 18.80 mmol) was dissolved in 85 mL acetic acid (AcOH). In an another flask, a solution of $NaNO_2$ (1.43 g, 20.72 mmol) in 30 mL H_2O was prepared and then added to solution of 3,6-dibromobenzene-1,2-diamine slowly. The mixture was stirred for 1 hour at room temperature after the addition completed. The precipitate was filtered and washed with distilled water many times. At the end, 4,7-dibromo-2H-benzo[d][1,2,3]triazole was obtained as a light pink powder. (3.0 g, yield 60%)

2.2.5. Synthesis of 4,7-dibromo-2-(2-octyldodecyl)-2H-benzo[d][1,2,3]triazole

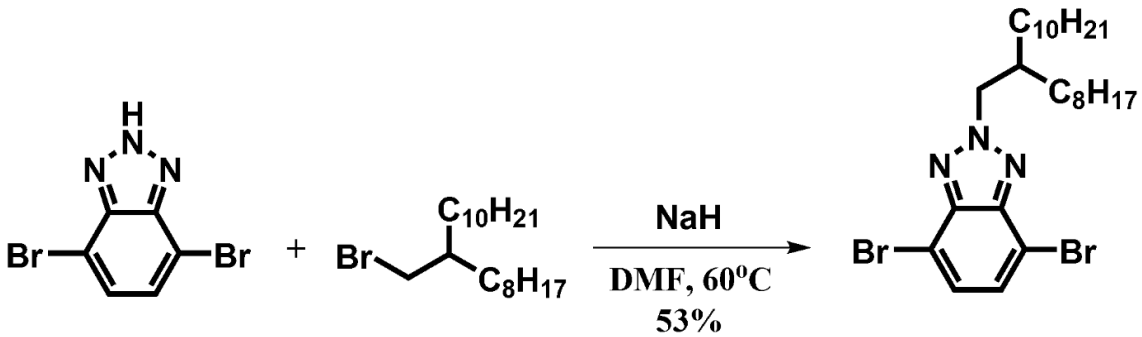

Figure 21. Synthesis of 4,7-Dibromo-2-(2-octyldodecyl)-2H-benzo[d][1,2,3]triazole

4,7-Dibromo-2H-benzo[d][1,2,3]triazole (2.36 g, 8.52 mmol) was put in a reaction flask under argon atmosphere. Then, 4,7-dibromo-2H-benzo[d][1,2,3]triazole was dissolved in dimethylformamide (DMF) (10 mL) and NaH (245 mg, 10.22 mmol) was added at room temperature. After dissolution of NaH, the reaction was heated to 70˚C. At that temperature, 9-(bromomethyl)nonadecane (3.70 g, 10.22 mmol) was added in one step. The reaction was stirred at 70˚C overnight. The residue was extracted with chloroform and water. The organic part was dried over $MgSO_4$ and then, evaporation of chloroform was done under reduced pressure. Column chromatography on silica gel with hexane and $CHCl_3$ (4:1) yielded 4,7- dibromo-2-(2-octyldodecyl)-2H-benzo[d][1,2,3]triazole as a yellow oil (2.5 g, yield 53%)

^{1}H NMR (400 MHz, $CDCl_3$), d (ppm): 7.36 (s, 2H), 4.62 (d, J= 7.3 Hz, 2H), 2.26 (m, 1H), 1.15(m, 32H), 0.80 (m, 6H). ^{13}C NMR (400 MHz, $CDCl_3$), d (ppm): 140.3, 128.2, 106.3, 56.6, 35.3, 29.3, 29.4, 29.3, 29.0, 27.5, 27.3, 27.2, 27.1, 27.0, 26.9, 23.5, 20.4, 20.3, 11.5.

2.3. Synthesis of Polymers

2.3.1. Synthesis of P1

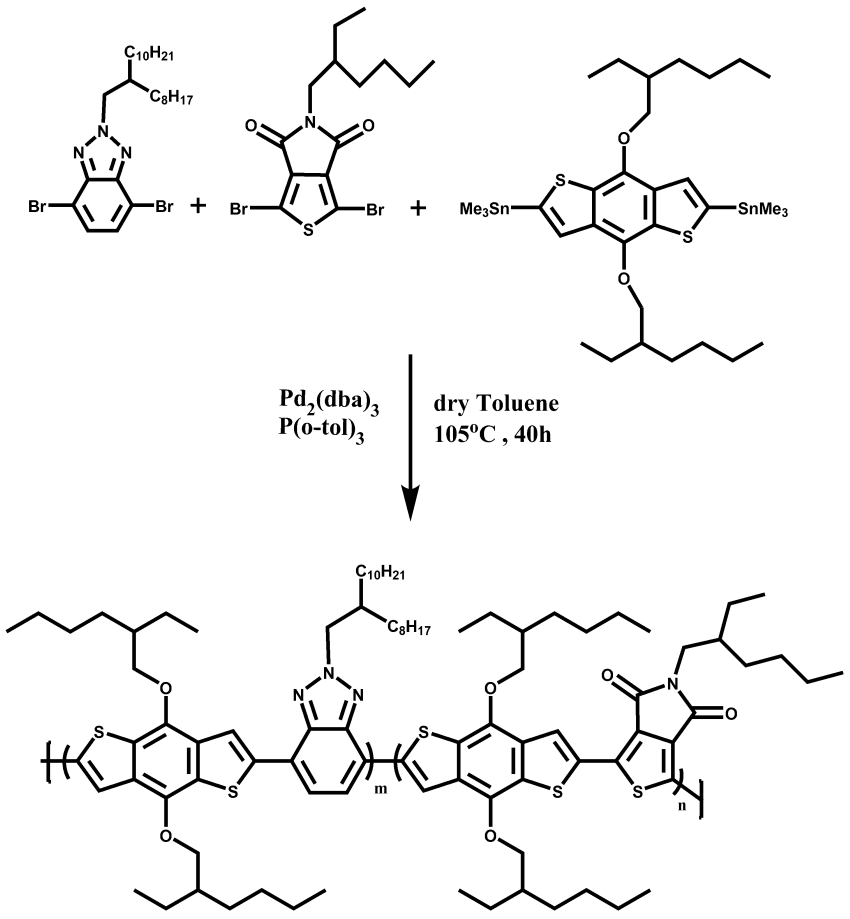

Figure 22. Synthetic Pathway for **P1**

4,7-Dibromo-2-(2-octyldodecyl)-2H-benzo[d][1,2,3]triazole (90.23 mg, 0.16 mmol), 1,3-dibromo-5-(2-ethylhexyl)-4*H*-thieno[3,4-*c*]pyrrole- 4,6(5*H*)-dione (68.49 mg, 0.16 mmol) and 4,8-bis((2-ethylhexyl)oxy)benzo[1,2-b:4,5-b’]dithiophene-2,6-diyl)bis(trimethylstannane) (250 mg, 0.32 mmol) were put in a rounded reaction flask and dissolved in dry toluene. The mixture was purged with argon for 30 min and then

$Pd_2(dba)_3$ (7.40 mg, 5% by mol) and tri-o-tolylphosphine (19.70 mg, 40% by mol) were added at the same time. The temperature was set as 105˚C. The mixture was stirred for 40 hours at that temperature. 2-Bromothiophene (52.77 mg, 0.32 mmol) was added as the first end-capper. The second end-capper, 2-tributylstanylthiophene (0.242 g, 0.320 mmol) was added after 3 hours. The reaction mixture was stirred for an additional 12 hours. The solvent was evaporated under reduced pressure. The residue was dissolved in $CHCl_3$ and precipitated into methanol. Then, it was washed with acetone. Polymer was extracted with hexane and precipitated into methanol to obtain dark purple solids (210 mg, yield 83%)

GPC; Number-average molecular weight (Mn) = 19 kDa, Polydispersity index (PDI) = 2.7

2.3.2. Synthesis of P2

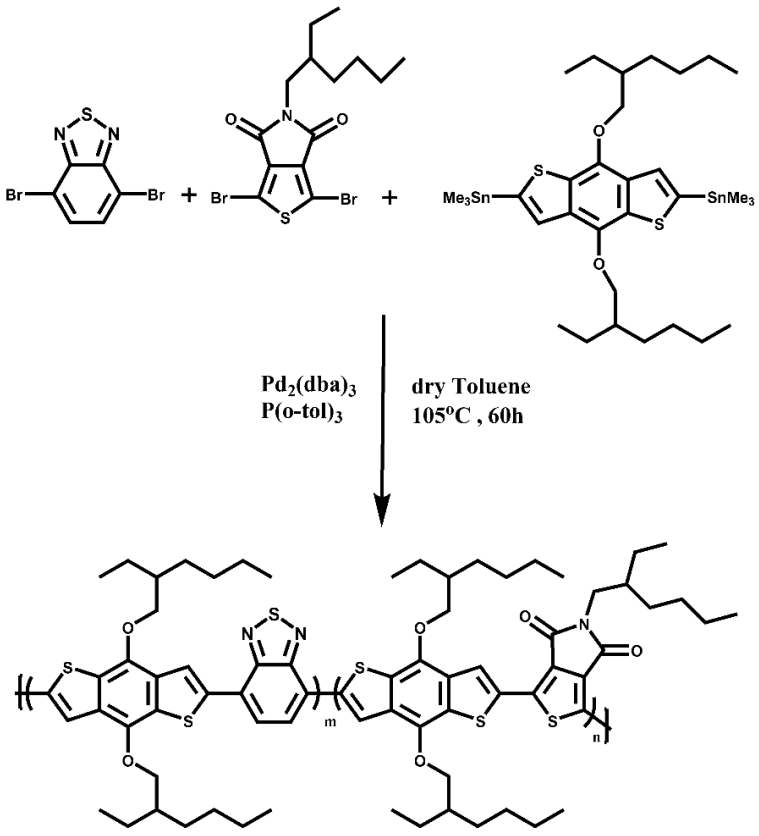

Figure 23. Synthetic Pathway for **P2**

4,7-Dibromobenzo[c][1,2,5]thiadiazole (47.60 mg, 0.16 mmol), 1,3-dibromo-5-(2-ethylhexyl)-4*H*-thieno[3,4-*c*]pyrrole- 4,6(5*H*)-dione (68.5 mg, 0.16 mmol) and 4,8-bis((2-ethylhexyl)oxy)benzo[1,2-b:4,5-b']dithiophene-2,6-diyl)bis(trimethylstannane) (250 mg, 0.32 mmol) were put in a rounded reaction flask and dissolved in dry toluene. The mixture was purged with argon for 30 min and then $Pd_2(dba)_3$ (7.4 mg, 5 % by mol) and tri-o-tolylphosphine (19.70 mg, 40 % by mol) were added at the same time. The temperature was set as 105˚C. The mixture was stirred for 60 hours at that temperature. 2-Bromothiophene (52.77 mg, 0.32 mmol) was added as the first end-capper. The second end-capper, 2-tributylstanylthiophene (0.242 g, 0.320 mmol) was added after 3 hours. The reaction mixture was stirred for an additional 12 hours. The solvent was evaporated under reduced pressure. The residue was dissolved in $CHCl_3$ and precipitated into methanol. Then, it was washed sequentially with acetone and hexane. Polymer was extracted with chloroform and precipitated into methanol to obtain dark blue solids (200 mg, yield 95 %)

GPC; Number-average molecular weight (Mn) = 166 kDa, Polydispersity index (PDI)=2.2

2.4. Characterization of Conducting Polymers

2.4.1. Gel Permeation Chromatography

Gel permeation chromatography (GPC) technique was used to determine molecular weight and polydispersity index (PDI) of polymers. The instrument was calibrated with polystyrene standards. Polymers were dissolved in THF (4.0 mg/mL) to determine molecular weight distribution of the polymers.

2.4.2. Thermal Analysis

Differential scanning calorimetry (DSC) and thermogravimetry analysis (TGA) were studied for investigation of the thermal analysis of the polymers. Under nitrogen atmosphere, Perkin Elmer Pyris 1 TGA was used for thermogravimetry analysis. The heating rate was 10 ^{o}C/min and decomposition temperature (T_d) was reported. Perkin Elmer DSC Diamond was used under nitrogen atmosphere with a 10 ^{o}C/min heating rate up to 500 ^{o}C in order to investigate glass transition temperature (T_g) and melting point (T_m) of the synthesized polymers.

2.4.3. Electrochemical Studies

Electrochemical studies were performed to investigate oxidation and reduction behaviors of polymers and to calculate their HOMO and LUMO energy levels by cyclic voltammetry (CV). Indium tin oxide (ITO) surfaces were coated by spray coating the polymers dissolved in chloroform. A three-electrode system comprising an ITO as the working electrode (WE), , platinum as the counter electrode (CE) and silver wire as the reference electrode (RE), was used. 0.1 M tetrabutylammonium hexafluorophosphate ($TBAPF_6$) in acetonitrile (ACN) solution were prepared in a quartz cuvette and then polymer coated ITO was dipped into the solution. By using Gamry Instrument Reference 600 Potentiostat, redox behaviors and color changes of polymers were determined. Then, current density versus applied voltage was plotted. HOMO level of the polymer was calculated from the onset potential of oxidation and LUMO level of the polymer was determined by the onset potential of reduction. The difference between HOMO and LUMO gives the electronic band gap of polymer.

2.4.4. Spectroelectrochemical Studies

Investigation of electrochromic properties of polymers was done via spectroelectrochemical studies. The determination of polaron and bipolaron bands of the polymers were investigated via studying their UV-Vis-NIR spectra. The spectra proved the color change in electrochemical studies and demonstrated maximum absorption wavelengths (λ_{max}) of polymers and information about optical band gaps (E_g^{op}). The optical band gap was calculated by taking a tangent line from the π-π* interband transition. The onset point (λ_{onset}) of that line was from the maximum absorption wavelength of polymer onsets and then optical band gap was calculated from the Eq. 5.

$$E_g^{op} = \frac{1241}{\lambda_{onset}} \qquad \textbf{Eq.5}$$

2.4.5. Kinetic Studies

The kinetic studies demonstrated the transmittance change with a time interval between maximum absorption wavelength of neutral and fully oxidized states of polymers. So, UV-Vis-NIR spectrophotometer was used to calculate optical contrasts of polymer. In addition to that, Chronoamperometry was used to determine the switching times of polymers.

2.4.6. Photovoltaic Studies

The bulk heterojunction organic solar cell devices were fabricated as following: ITO coated glass substrates were cleaned in an ultrasonic bath for 15 minutes with toluene, detergent, water, acetone and isopropyl alcohol after etching with HCl. Then, Harrick Plasma Cleaner for oxygen plasma treatment was used to dispose of any remaining organic component. PEDOT: PSS was coated onto ITO surface by spin coating at different rpm values. Afterwards, in order to evaporate water, substrates were dried at 130˚C for 15 minutes. Active layer of the solar cell was obtained via dissolving

synthesized polymers and $PC_{71}BM$ with different ratio in different solvents like chloroform, chlorobenzene and dichlorobenzene. Polytetrafluoroethylene (PTFE) syringe was utilized for the filtration of polymer: $PC_{71}BM$ mixtures with the purpose of having a homogenous solution. Then, the mixture of polymer:$PC_{71}BM$ was coated onto ITO surface before evaporation of LiF and Al layers. Finally, Current density-voltage characteristics were tested using Keithley 2400 under illumination of Atlas Material Testing Solutions solar simulator (AM 1.5 G).

CHAPTER 3

3. RESULTS & DISCUSSION

3.1. Electrochemical Studies

Electrochemical studies were investigated using cyclic voltammetry in order to study HOMO-LUMO energy levels of the corresponding polymers and their band gaps. Since these studies provide the information on the character of synthesized polymers whether they are proper for the organic photovoltaic applications or not. After the polymers were dissolved in chloroform, they were coated onto ITO coated glass surfaces through spray coating technique. The three-electrode system was prepared with the purpose of observing oxidation and reduction potentials of the polymers. The three-electrode system was made up of platinum wire, silver wire and polymer coated ITO substrate in quartz cell which is containing $TBAPF_6$/ACN electrolyte solution. Cyclic voltammograms with a scan rate of 100 mV/s proved that both polymers have ambipolar character which means that the polymers were both n and p dopable. The p-type doping and dedoping peaks of **P1** and **P2** were calculated as 1.04 V/0.84 V and 1.12 V/0.86 V. On the other hand, **P1** had an n-type doping peak at -1.58 V and one n-type dedoping peak at -1.44 V. Moreover, the n type doping and dedoping peaks for **P2** were -1.64/-1.34, correspondingly. The cyclic voltammograms of these two polymers were demonstrated in Figure 24.

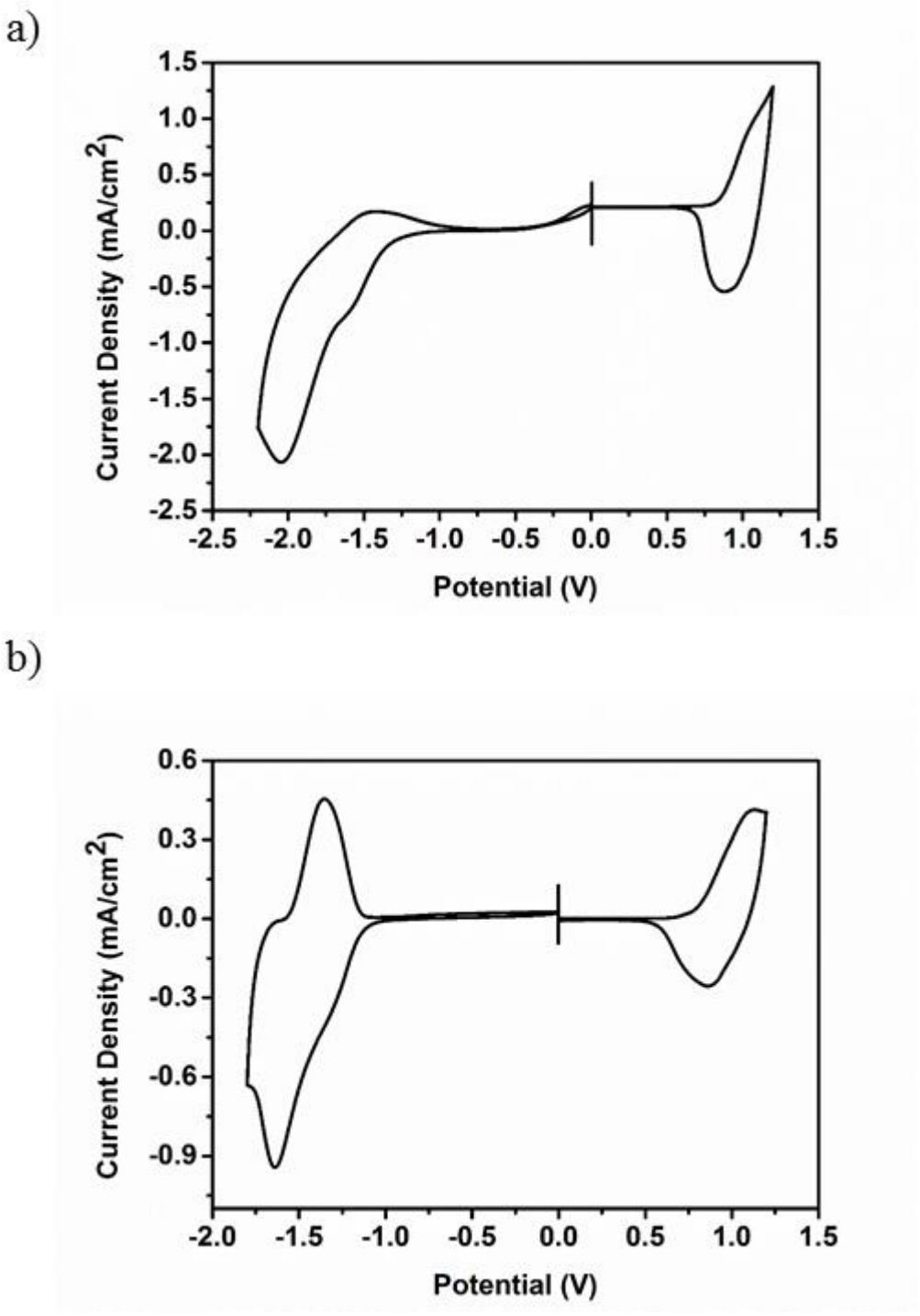

Figure 24. Single-scan Cyclic Voltammograms of Polymer Films in 0.1 M $TBAPF_6$ / ACN Electrolyte Solution (a) **P1** (b) **P2**

If a polymer has both p- and n-dopable character, HOMO and LUMO energy levels of the polymers can be calculated from the following equations (Eq. 6) via cyclic voltammograms.

$$HOMO = -(4.75 + E_{ox,onset})$$
$$LUMO = -(4.75 + E_{red,onset}) \quad \textbf{Eq.6}$$

From the tangent lines of the doping peaks, the onset potentials of oxidation and reduction were calculated. Thus, HOMO and LUMO energy levels of **P1** were calculated as -5.53 eV and -3.43 eV, respectively. However, HOMO energy level of **P2** was -5.54 eV, whereas -3.53 eV was recorded as LUMO energy level of **P2**. Further, electronic band gap (E_g^{el}) of the polymers were obtained from the formula below (Eq.7) and E_g^{el} values were found as 2.10 eV and 2.01 eV for **P1** and **P2,** sequentially.

$$E_g^{el} = HOMO - LUMO \quad \textbf{Eq.7}$$

The results of electrochemical studies were summarized in Table 1.

Table 1. Summary of Electrochemical Properties

	$E_{p\text{-doping}}$ (V)	$E_{p\text{-dedoping}}$ (V)	$E_{n\text{-doping}}$ (V)	$E_{n\text{-dedoping}}$ (V)	HOMO (eV)	LUMO (eV)	E_g^{ec} (eV)
P1	1.04	0.89	-1.58	-1.44	-5.53	-3.43	2.10
P2	1.12	0.86	-1.64	-1.35	-5.54	-3.53	2.01

P2 has benzothiadiazole moiety differs than **P1** that contains benzotriazole moiety. Due to the effect of benzothiadiazole on polymer backbone, **P2** has lower LUMO energy level.[60]

3.2. Spectroelectrochemical Studies

As shown in Figure 25, the light absorption behaviors of the synthesized polymers in UV-Vis-NIR regions were investigated as a function of wavelength. In this figure, the absorption peaks were observed 508 and 551 nm for **P1** while **P2** exhibited an absorption peak at 590 nm. These absorption peaks in the visible region pointed out π-π^* transition between HOMO and LUMO energy levels of polymers. Thus, **P2** showed red shift absorption compared to **P1** because of the increase in the conjugation length. The calculations of the optical band gap (E_g^{op}) of polymers were done by using the onset values of wavelengths (λ_{onset}). From the Eq.5, optical band gap values of **P1** and **P2** were obtained via using the maximum onset wavelengths values, 614 and 693 nm, as 2.02 eV and 1.79 eV, respectively. The lower band gap of the **P2** resulted from the red shift in the absorption. In addition to that, **P2** may harvest more visible light owing to its higher absorption edge. [61] The results of spectroelectrochemical studies were summarized in Table 2. The results showed that the optical band gaps of the polymers were lower than the electronic ones owing to the creation of free charge in cyclic voltammetry.[62]

Table 2. Summary of Spectroelectrochemical Studies

	λmax (nm)	**E_g^{op} (eV)**
P1	551/508	2.02
P2	590	1.79

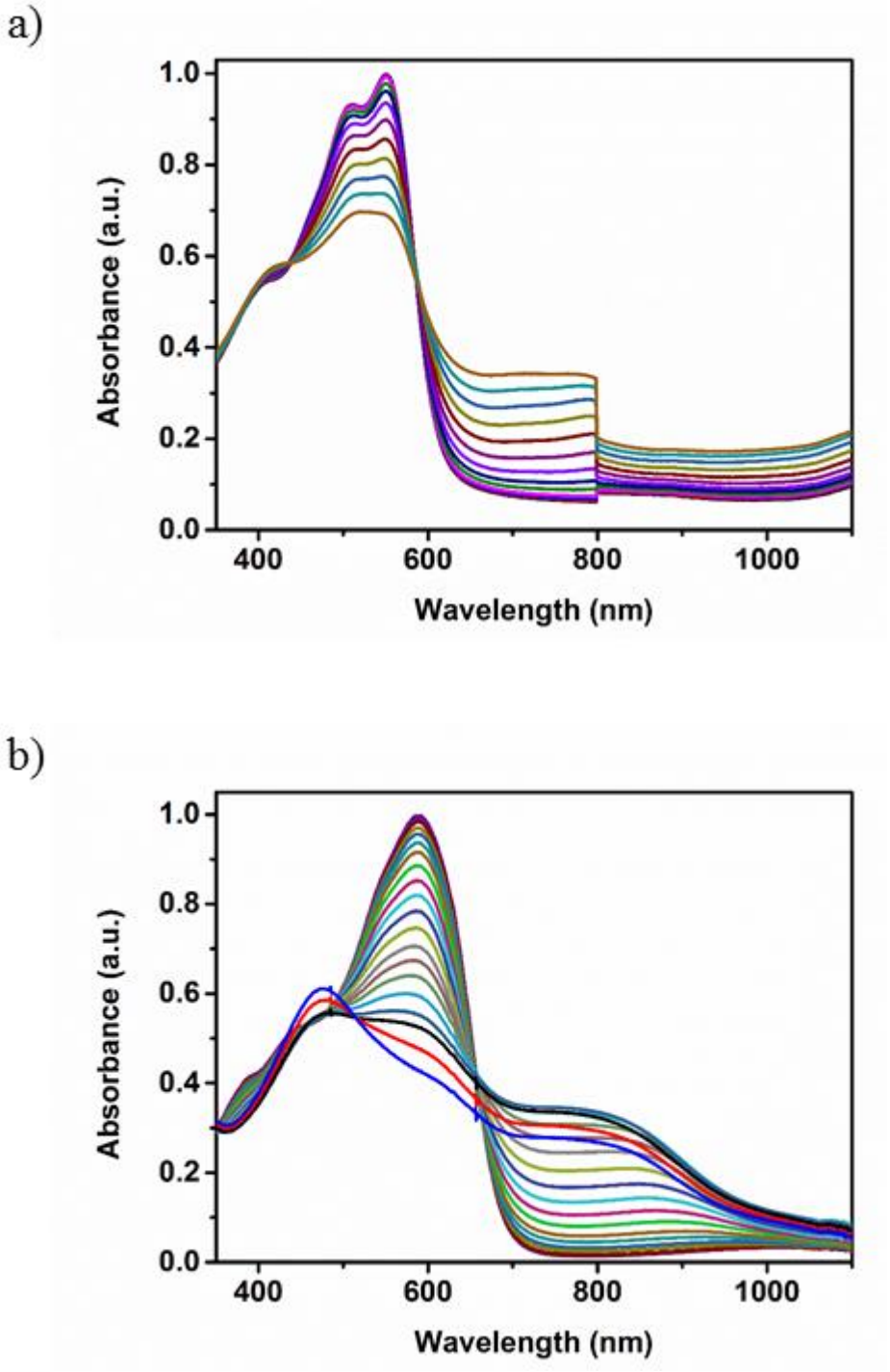

Figure 25. UV-Vis-NIR Spectra of a) **P1** and b) **P2** in 0.1 M $TBAPF_6$ / ACN Electrolyte Solution

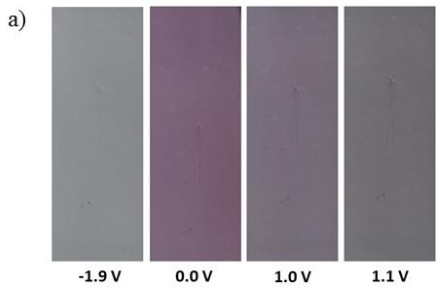

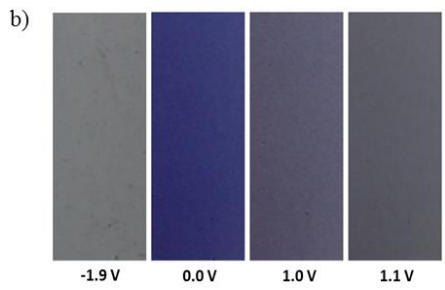

	-1.9 V	0.0 V	1.0 V	1.1 V
L	59	43	48	47
a	0	13	6	3
b	-2	-7	-5	-3

	-1.9 V	0.0 V	1.0 V	1.1 V
L	51	28	39	41
a	0	13	5	2
b	-1	-33	-12	-6

Figure 26. The Colors of a) **P1** and b) **P2** with their L, a and b Values

The colors of the polymers were established by International Commission on Illumination (CIE) system. The system based on luminance (L), hue (a) and saturation (b) and depicted in Figure 26. Both polymers demonstrated different colors between their neutral, oxidized and reduced states. **P1** exhibited purple color in neutral state while **P2** had dark blue color in that state. Both polymers showed dark grey in oxidized state and light grey in reduced state.

As shown in Figure 27, polymers exhibited broad absorption in visible region. **P1** had a two absorption peaks that may be assigned to π-π^* transition and intermolecular charge transfer. Moreover, the absorption spectra of **P1** were red shifted in comparison with its polymer solution because of aggregation and interactions between the main chains of polymer in the solid state.[63]

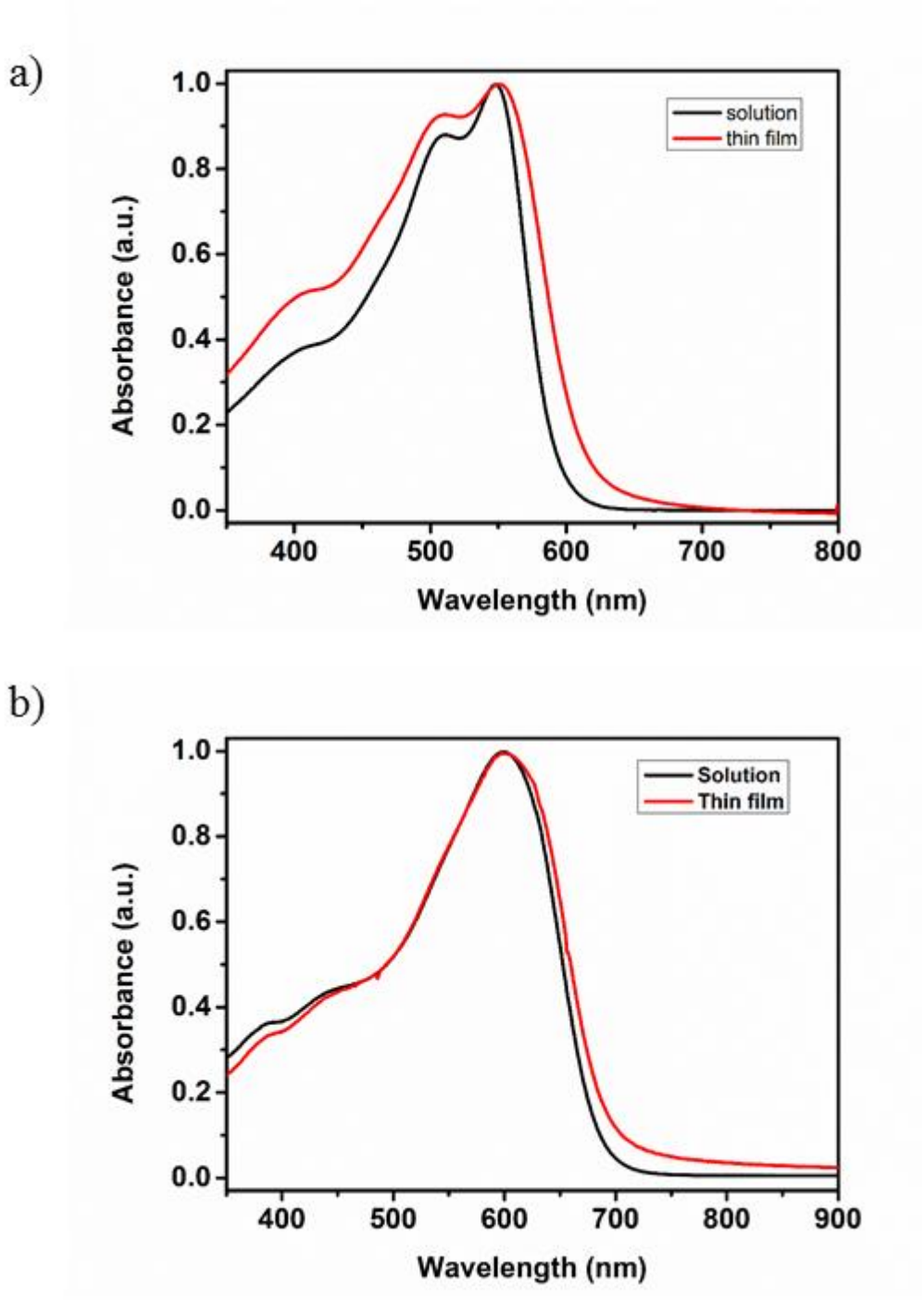

Figure 27. Absorption Spectra of (a) **P1**, (b) **P2** in Thin Film and Chloroform Solution

3.3. Kinetic Studies

Kinetic studies were investigated in order to have information on the percent transmittance changes and switching times of polymers between their neutral and fully oxidized states. For that purpose, maximum wavelengths of the polymers were chosen and voltages were varied between 0.0 V-1.1 V for **P1** and 0.0 V- 1.1 V for **P2**. The percent transmittance changes were determined for each polymer. The percent transmittance changes were calculated based on the sensitivity of human eye which is accepted as 95 % of the full contrast. Optical contrast values of **P1** were achieved as 19 % (550 nm) and 34 % (720 nm). In addition, **P2** exhibited optical contrast values of 23 % (590 nm) and 22 % (760 nm). Switching times of **P1** were noted as 2.6 s (550 nm) and 0.6 s (720 nm). On the other hand, the switching times values for **P2** were 2.2 s (590 nm) and 1.1 s (760 nm). The results of kinetic studies were summarized in Table 3.

Table 3. Summary of Kinetic Studies

	Optical contrast (ΔT %)		**Switching times (s)**
P1	19	550 nm	2.6
	34	720 nm	0.6
P2	23	590 nm	2.2
	22	760 nm	1.1

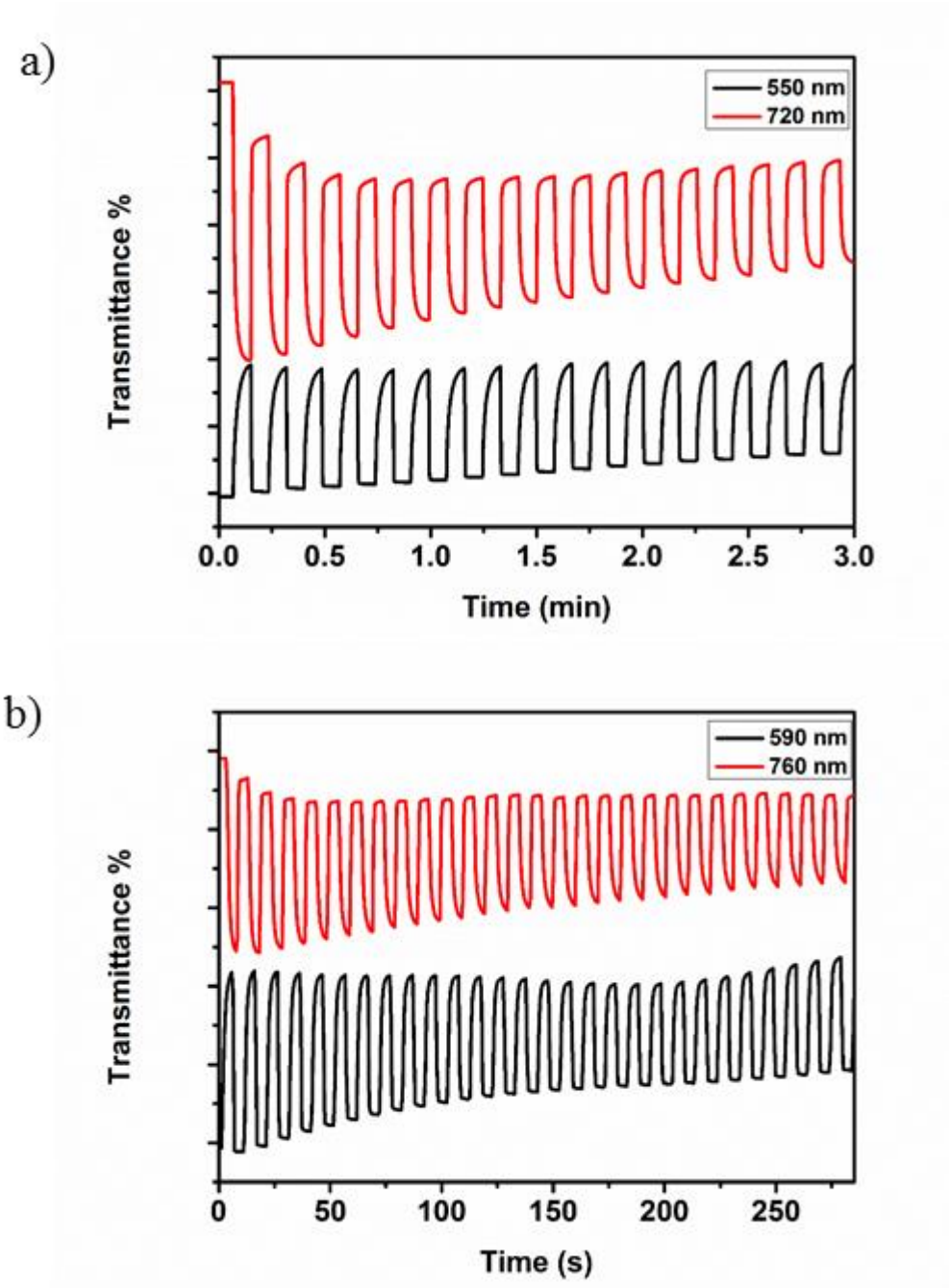

Figure 28. Percent Transmittance Change of (a) **P1** (b) **P2** in 0.1 M $TBAPF_6$ / ACN Electrolyte Solution at Maximum Wavelengths of Polymers

3.4. Thermal Analyses of Polymers

TGA and DSC were used to perform thermogravimetry analyses of polymer under inert nitrogen atmosphere. Although 53 % mass loss was examined at 650 °C for **P1**, **P2** has a mass loss as 22 % at 700 °C. **P1** and **P2** did not reveal any glass-transition temperature (T_g). TGA and DSC analysis results were shown in **Appendix A**.

3.5. Organic Solar Cell Device Applications

Bulk heterojunction organic solar cell applications of ITO/PEDOT:PSS/Polymer: $PC_{71}BM$/LiF/Al device was investigated with AM 1.5G illumination after electrochemical studies showed that these polymers had proper HOMO and LUMO energy levels and band gaps. Figure 29 represents the energy levels of the materials which were used in OSC device fabrication.

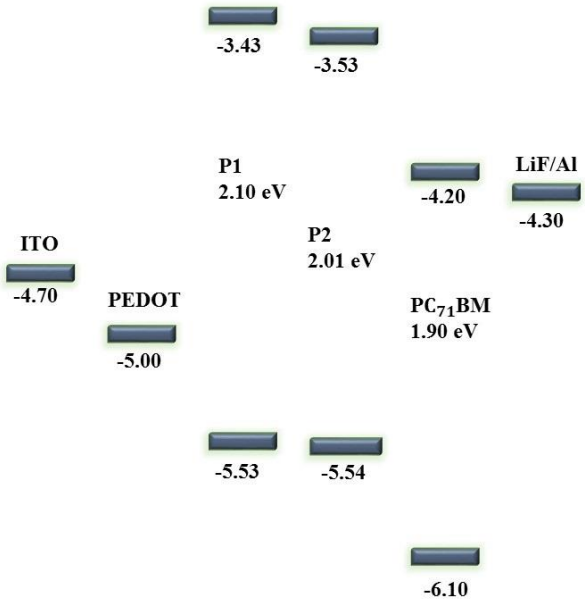

Figure 29. The Energy Levels of Materials Used in Bulk Heterojunction Organic Solar Cell Device Fabrication

Synthesized polymers were used as the donor materials and $PC_{71}BM$ moiety was chosen as the acceptor material since it increases absorption in the visible region from 440 nm to 530 nm.[64] A mixture of polymer:PCBM in different weight to weight ratios

was introduced onto PEDOT:PSS coated surface as the active layer. As PCBM amount was increased ability of electron transport also increased which resulted in better short circuit current and PCE. In contrast, decreasing the polymer amount can cause lowering of short circuit current and also of PCE due a decrease in collected photons. Hence, ratio of polymer:PCBM is very significant and therefore it should be optimized. Furthermore, power conversion efficiency is affected by thickness of the active layer, morphology, molecular weight of synthesized polymers, and solvent which is used for dissolving of polymer: PCBM mixture. After these optimizations were carried out, current density-voltage characteristics were drawn and power conversion efficiency of devices were calculated. The highest PCE for **P1** was achieved as 2.55 % for **P1**:$PC_{71}BM$ (1:3, w/w). On the other hand, the maximum power conversion efficiency was 5.83 % for **P2**:$PC_{71}BM$ (1:2, w/w). Summary of best results of photovoltaic studies for both polymers was shown in the Tables 4 and 5.

Table 4. Summary of Photovoltaic Studies of **P1**

Polymer:$PC_{71}BM$	**%**	**V_{oc} (V)**	**J_{sc} (mA/cm^2)**	**FF (%)**	**η (%)**	**Polymer (rpm)**
P1 (1:1)	2	0.83	1.49	68	0.84	500
P1 (1:2)	2	0.82	2.48	60	1.22	500
P1 (1:3)	2	0.84	4.09	62	2.14	500
P1 (1:3)	2	0.84	4.75	64	2.55	750
P1 (1:4)	2	0.78	2.67	60	1.25	500

Table 5. Summary of Photovoltaic Studies of **P2**

Polymer:$PC_{71}BM$	**%**	**V_{oc} (V)**	**J_{sc} (mA/cm^2)**	**FF (%)**	**η (%)**	**Polymer (rpm)**
P2 (1:1)	2	0.74	9.07	54	3.62	500
P2 (1:2)	2	0.71	11.22	60	4.78	500
P2 (1:3)	2	0.71	7.53	55	2.94	500
P2 (1:4)	2	0.70	8.16	60	3.42	500
P2 (1:1)	3	0.80	13.15	45	4.73	750
P2 (1:2)	3	0.80	14.02	52	5.83	750

V_{oc} values for **P1** varied between 0.78-0.84 V, while open circuit voltage values of **P2** were between 0.71-0.80 V. Although **P1** had higher V_{oc} values, organic photovoltaic device of **P2** demonstrated much more power conversion efficiency owing to its much better short circuit current (J_{sc}) values. In addition to these, fill factor (FF) values of **P1** were observed between 60-68 %, while **P2** had a range between 45-60 %. These values were calculated from the current density voltage graphs of the polymers and the graphs of best results were shown in Figure 30.

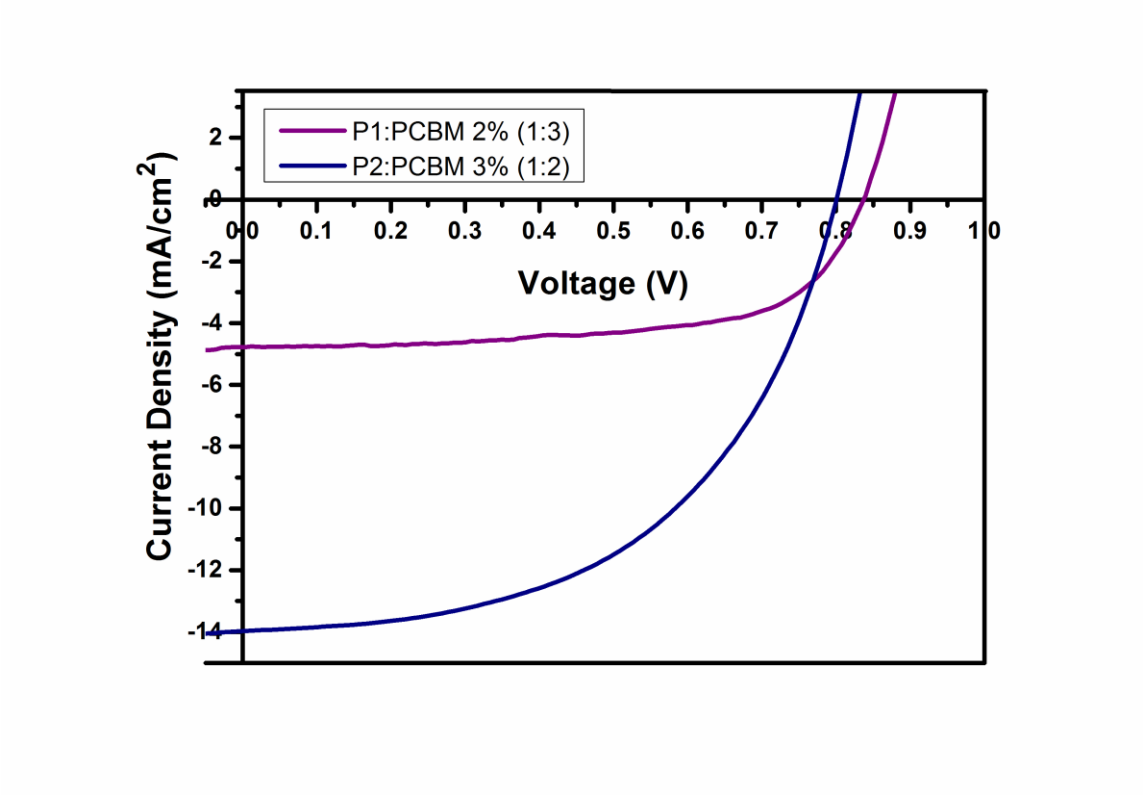

Figure 30. Current Density-Voltage (J-V) Characteristics of **P1** and **P2** of the Best Devices

Incident photon to current efficiency (IPCE) was used in order to investigate the ratio of number of charges collected by electrodes to the number of incident photons. The photo response of the best devices is shown in Figure 31. Photocurrent response for both polymer was performed between 350 nm to 900 nm. The highest IPCE value for **P1** and **P2** reached 23 % and 58 %, respectively.

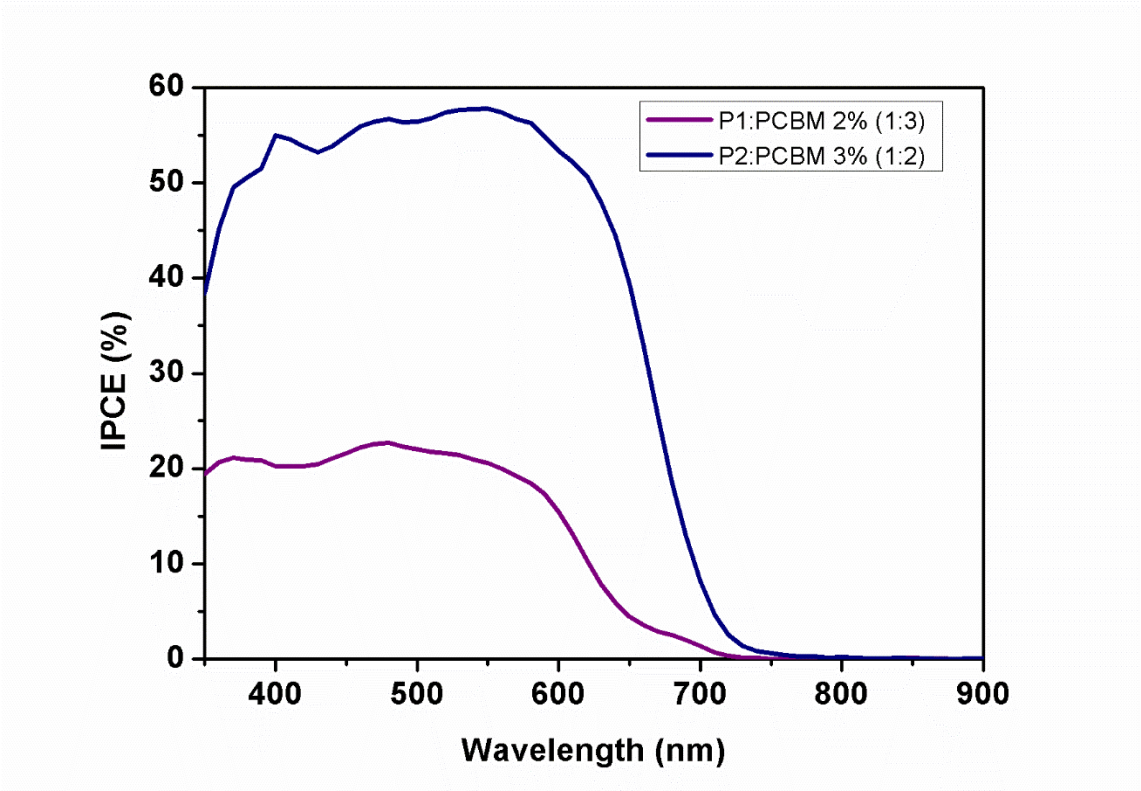

Figure 31. IPCE Curve for the Best Performance Solar Cells

3.6. Morphology

Device performance of an OSC is affected by morphology of polymer:PCBM blends. In order to have information about the morphology of these devices, atomic force microscopy (AFM) and transmission electron microscopy (TEM) were utilized. AFM and TEM images of the most efficient devices are shown in Figure 32. Roughness of the blends were examined via using AFM and reported as 9.77 nm and 1.78 nm for **P1**:$PC_{71}BM$ (1:3) and **P2**:$PC_{71}BM$ (1:2), respectively. Surface roughness of active layers is related with J_{sc}. While roughness decreases, J_{sc} is increases and then higher PCE can be achieved. This smooth surface of **P2**:$PC_{71}BM$ (1:2) may be a reason for a better device performance.

Besides AFM, TEM images were studied in order to gain more insight on the morphology for both polymer:PCBM blends. The dark and bright areas in the TEM

are contributions from PCBM rich domains and polymer rich domains, respectively. Since, PCBM domains should appear darker in TEM images due to its high electron density. The blend film of **P1**:$PC_{71}BM$ showed larger domains than that of **P2**:$PC_{71}BM$ and that may limit device performance.

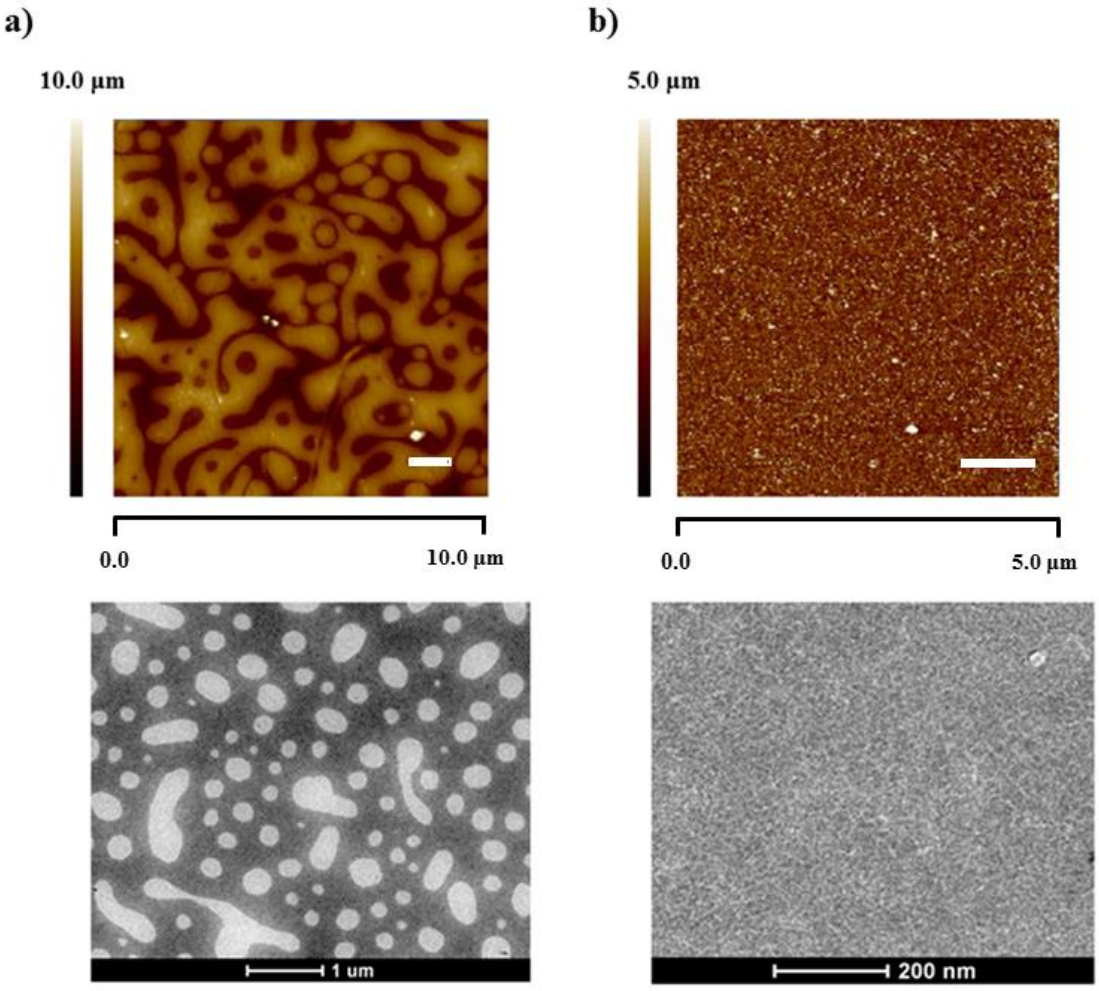

Figure 32. AFM and TEM Images of a) **P1**:$PC_{71}BM$ (1:3) and b) **P2**:$PC_{71}BM$ (1:2). Scale Bars in AFM Images are 1µm.

CHAPTER 4

4. CONCLUSIONS

In this study benzodithiophene and thienopyrroledione containing random conjugated polymers **P1** and **P2** were synthesized via Stille coupling in order to investigate the effect of benzotriazole and benzothiadiazole moieties on optoelectronic and photovoltaic properties. **P1** and **P2** were used in the active layer of organic solar cell devices after blending with $PC_{71}BM$. Electrochemical studies represented that **P1** and **P2** have both n-and p- dopable characters. Thus, electronic band gap (E_g^{el}) of the polymers were found as 2.10 eV and 2.01 eV for **P1** and **P2,** respectively. The optical band gap values of **P1** and **P2** were obtained via using the maximum onset wavelengths values; 614 and 693 nm as 2.02 eV and 1.79 eV, respectively. The lower band gap of the **P2** resulted from the red shift in the absorption. Optical contrast values of **P1** achieved as 19 % (550 nm) and 34 % (720 nm), while **P2** exhibited optical contrast values of 23 % (590 nm) and 22 % (760 nm). Switching times of **P1** were noted as 2.6 s (550 nm) and 0.6 s (720 nm). On the other hand, the switching times values for **P2** were 2.2 s (590 nm) and 1.1 s (760 nm). Electrochemical and optical experiments revealed that polymers are proper for organic solar cell applications owing to their proper HOMO and LUMO energy levels and low band gaps.

Bulk heterojunction organic solar cells with a device structure ITO/PEDOT:PSS/Polymer: $PC_{71}BM$/LiF/Al were constructed and investigated to obtain current density voltage characteristics of devices under AM 1.5G illumination. Mainly, owing to the improvement of J_{sc}, PCE of devices were reached to 2.55 % and 5.83 % for **P1** and **P2**, respectively. The highest PCE of **P1** was obtained with a V_{oc} of 0.84 V, a J_{sc} of 4.75 mA/cm^2, and a FF of 64 %. On the other hand, **P2** showed the best results with a V_{oc} of 0.80 V, a J_{sc} of 14.02 mA/cm^2, and a FF of 52 %.

5. REFERENCES

(1) Kar, P. *Doping in Conjugated Polymers*; John Wiley & Sons, Ltd, 2013.

(2) Harun, M. H.; Saion, E.; Kassim, A.; Yahya, N.; Mahmud, E. *Sensors Peterbrgh. NH* **2007**, *2* (May 2016), 63–68.

(3) Baran, D.; Balan, A.; Celebi, S.; Meana Esteban, B.; Neugebauer, H.; Sariciftci, N. S.; Toppare, L. *Chem. Mater.* **2010**, *22* (9), 2978–2987.

(4) Liming Dai. *Intelligent Macromolecules for Smart Devices:From Materials Synthesis to Device Applications*; 2004.

(5) Bakhshi, A. K.; Bhalla, G. *J. Sci. Ind. Res.* **2004**, *63* (September), 715–728.

(6) Bredas, J.L., Scott, J.C., Yakushi, K., Street, G. B. *Phyiscal Rev. B* **1984**, *30* (2), 1023–1025.

(7) Bredas, J.; Street, G. *Acc. Chem. Res.* **1985**, *1305* (4), 309–315.

(8) Nunzi, J.-M. *Comptes Rendus Phys.* **2002**, *3* (4), 523–542.

(9) Zhou, H.; Yang, L.; You, W. *Macromolecules* **2012**, *45*, 607–632.

(10) Waltman, R. J.; Bargon, J.; Diaz, a F. *J. Phys. Chem.* **1983**, *87* (8), 1459–1463.

(11) Cheng, Y.-J.; Yang, S.-H.; Hsu, C.-S. *Chem. Rev. (Washington, DC, U. S.)* **2009**, *109* (11), 5868–5923.

(12) Brabec, C. J.; Winder, C.; Sariciftci, N. S.; Hummelen, J. C. *Adv. Funct. Mater.* **2002**, No. 12, 709–712.

(13) Roncali, J. *Macromol. Rapid Commun.* **2007**, *28* (17), 1761–1775.

(14) Zgou, H.; Zahlou, A. *Int. J. Adv. Res. Comput. Sci. Softw. Eng.* **2014**, *4* (5), 10-19.

(15) Havinga, E. E.; ten Hoeve, W.; Wynberg, H. *Synth. Met.* **1993**, *55* (1), 299–306.

(16) Zhang, Z.; Wang, J. *J. Mater. Chem.* **2012**, *22* (10), 4178.

(17) Guo, X.; Ortiz, R. P.; Zheng, Y.; Kim, M.-G.; Zhang, S.; Hu, Y.; Lu, G.; Facchetti, A.; Marks, T. J. *J. Am. Chem. Soc.* **2011**, *133* (34), 13685–13697.

(18) Yuan, M.-C.; Chiu, M.-Y.; Liu, S.-P.; Chen, C.-M.; Wei, K.-H. *Macromolecules* **2010**, *43* (17), 6936–6938.

(19) Alqurashy, B. A.; Iraqi, A.; Zhang, Y.; Lidzey, D. G. *Eur. Polym. J.* **2016**, *85*, 225–235.

(20) Su, Y.-W.; Lan, S.-C.; Wei, K.-H. *Mater. Today* **2012**, *15* (554), 554–562.

(21) Tanimoto, A.; Yamamoto, T. *Macromolecules* **2006**, *39* (10), 3546–3552.

(22) Gedefaw, D.; Tessarolo, M.; Bolognesi, M.; Prosa, M.; Kroon, R.; Zhuang, W.; Henriksson, P.; Bini, K.; Wang, E.; Muccini, M.; Seri, M.; Andersson, M. R. *Beilstein J. Org. Chem.* **2016**, *12*, 1629–1637.

(23) Murugesan, V.; de Bettignies, R.; Mercier, R.; Guillerez, S.; Perrin, L. *Synth. Met.* **2012**, *162* (11–12), 1037–1045.

(24) Min, J.; Zhang, Z.-G.; Zhang, S.; Zhang, M.; Zhang, J.; Li, Y. *Macromolecules* **2011**, *44* (19), 7632–7638.

(25) Chen, Y.; Yan, Y.; Du, Z.; Bao, X.; Liu, Q.; Roy, V. a. L.; Sun, M.; Yang, R.; Lee, C. S. *J. Mater. Chem. C* **2014**, *2*, 3921.

(26) Ledwon, P.; Zassowski, P.; Jarosz, T.; Lapkowski, M.; Wagner, P.; Cherpak, V.; Stakhira, P. *J. Mater. Chem. C* **2016**, *4* (11), 2219–2227.

(27) Liu, Y.; Chen, C.-C.; Hong, Z.; Gao, J.; Yang, Y. M.; Zhou, H.; Dou, L.; Li, G.; Yang, Y. *Sci. Rep.* **2013**, *3*, 3356.

(28) Reddy Busireddy, M.; Niladri, V.; Mantena, R.; Chereddy, N. R.; Shanigaram, B.; Kotamarthi, B.; Biswas, S.; Sharma, G. D.; Vaidya, J. R. *Org. Electron.* **2016**, *37*, 312–325.

(29) Zhang, Y.; Hau, S. K.; Yip, H. L.; Sun, Y.; Acton, O.; Jen, A. K. Y. *Chem. Mater.* **2010**, *22* (9), 2696–2698.

(30) Gong, X.; Li, G.; Li, C.; Zhang, J.; Bo, Z. *J. Mater. Chem. A* **2015**, *3* (40), 20195–20200.

(31) Zhang, L.; He, C.; Chen, J.; Yuan, P.; Huang, L.; Zhang, C.; Cai, W.; Liu, Z.; Cao, Y. *Macromolecules* **2010**, *43* (23), 9771–9778.

(32) Skotheim;, T. A.; Reynolds, J. R. *Conjugated Polymers: Processing and Applications*; 2006.

(33) Argun, A. A.; Aubert, P.-H.; Thompson, B. C.; Schwendeman, I.; Gaupp, C. L.; Hwang, J.; Pinto, N. J.; Tanner, D. B.; MacDiarmid, A. G.; Reynolds, J. R. *Chem. Mater.* **2004**, *16* (23), 4401–4412.

(34) Mortimer, R. J. *Chem. Soc. Rev.* **1997**, *26*, 147–156.

(35) Chamberlain, G. A. *Sol. Cells* **1983**, *8* (1), 47–83.

(36) Wöhrle, D.; Meissner, D. *Adv. Mater.* **1991**, *3* (3), 129–138.

(37) Tang, C. W. *Appl. Phys. Lett.* **1986**, *48* (2), 183–185.

(38) Yu, G.; Gao, J.; Hummelen, J. C.; Wudl, F.; Heeger, A. J. *Science (80-.).* **1995**, *270* (5243), 1789–1791.

(39) Brabec, C. J.; Cravino, A.; Meissner, D.; Sariciftci, N. S.; Fromherz, T.; Rispens, M. T.; Sanchez, L.; Hummelen, J. C. *Adv. Funct. Mater.* **2001**, *11* (5), 374–380.

(40) Kugler, T.; Salaneck, W. R.; Rost, H.; Holmes, A. B. *Chem. Phys. Lett.* **1999**, *310* (5–6), 391–396.

(41) Günes, S.; Neugebauer, H.; Sariciftci, N. S. *Chem. Rev.* **2007**, *107* (4), 1324–1338.

(42) Clarke, T. M.; Durrant, J. R. *Chem. Rev.* **2010**, *110* (11), 6736–6767.

(43) Ganesamoorthy, R.; Sathiyan, G.; Sakthivel, P. *Sol. En. Mat. Sol. C.* **2016**, *161*, 102–148.

(44) Khalil, A.; Ahmed, Z.; Touati, F.; Masmoudi, M. In *2016 13th International Multi-Conference on Systems, Signals & Devices (SSD)*; IEEE, 2016; pp 342–353.

(45) Kaur, N.; Singh, M.; Pathak, D.; Wagner, T.; Nunzi, J. M. *Synth. Met.* **2014**, *190*, 20–26.

(46) Brédas, J.-L.; Norton, J. E.; Cornil, J.; Coropceanu, V. *Acc. Chem. Res.* **2009**, *42* (11), 1691–1699.

(47) Blom, P. W. M.; Mihailetchi, V. D.; Koster, L. J. A.; Markov, D. E. *Adv. Mater.* **2007**, *19* (12), 1551–1566.

(48) Deibe, C.; Strobe, T.; Dyakonov, V. *Adv. Mater.* **2010**, *22* (37), 4097–4111.

(49) Benanti, T. L.; Venkataraman, D. *Photosynth. Res.* **2006**, *87* (1), 73–81.

(50) Heeger, A. J. *Adv. Mater.* **2014**, *26* (1), 10–28.

(51) Qi, B.; Wang, J. *J. Mater. Chem.* **2012**, *22* (46), 24315.

(52) Scharber, M. C.; Mühlbacher, D.; Koppe, M.; Denk, P.; Waldauf, C.; Heeger, A. J.; Brabec, C. J. *Adv. Mater.* **2006**, *18* (6), 789–794.

(53) Wright, M.; Uddin, A. *Sol. En. Mat. Sol. C.* **2012**, *107*, 87–111.

(54) Zou, Y.; Najari, A.; Berrouard, P.; Beaupre, S.; Aïch, B. R.; Tao, Y.; Leclerc, M. *J. Am. Chem. Soc.* **2010**, *132* (15), 5330–5331.

(55) Yuan, J.; Huang, X.; Zhang, F.; Lu, J.; Zhai, Z.; Di, C.; Jiang, Z.; Ma, W. *J. Mater. Chem.* **2012**, *22* (42), 22734.

(56) Unay, H.; Unlu, N. A.; Hizalan, G.; Hacioglu, S. O.; Yildiz, D. E.; Toppare, L.; Cirpan, A. *J. Polym. Sci. Part A Polym. Chem.* **2014**, *53* (4), 528–535.

(57) Hou, J.; Park, M.; Zhang, S.; Yao, Y.; Chen, L.-M.; Li, J.-H.; Yang, Y.

Macromolecules **2008**, *41* (16), 6012–6018.

(58) Aïch, B. R.; Lu, J.; Beaupré, S.; Leclerc, M.; Tao, Y. *Org. Electron. physics, Mater. Appl.* **2012**, *13* (9), 1736–1741.

(59) Liu, W.; He, D.; Qiu, B.; Jiang, L.; Chen, G.; Peng, H.; Zou, Y. *J. Macromol. Sci. Part A* **2015**, *52* (9), 752–760.

(60) Neto, B. A. D.; Lapis, A. A. M.; da Silva Júnior, E. N.; Dupont, J. *Euro. J. Org. Chem.* **2013**, *2013* (2), 228–255.

(61) Istanbulluoglu, C.; Göker, S.; Hizalan, G.; Hacioglu, S. O.; Udum, Y. A.; Yildiz, E. D.; Cirpan, A.; Toppare, L. *New J. Chem.* **2015**, *39* (8), 6623–6630.

(62) Cevher, S. C.; Unlu, N. A.; Ozelcaglayan, A. C.; Apaydin, D. H.; Udum, Y. A.; Toppare, L.; Cirpan, A. *J. Polym. Sci. Part A Polym. Chem.* **2013**, *51* (9), 1933–1941.

(63) Kim, J. H.; Kim, H. U.; Lee, J. K.; Park, M. J.; Hyun, M. H.; Hwang, D. H. *Synth. Met.* **2013**, *179*, 18–26.

APPENDIX A

NMR DATA

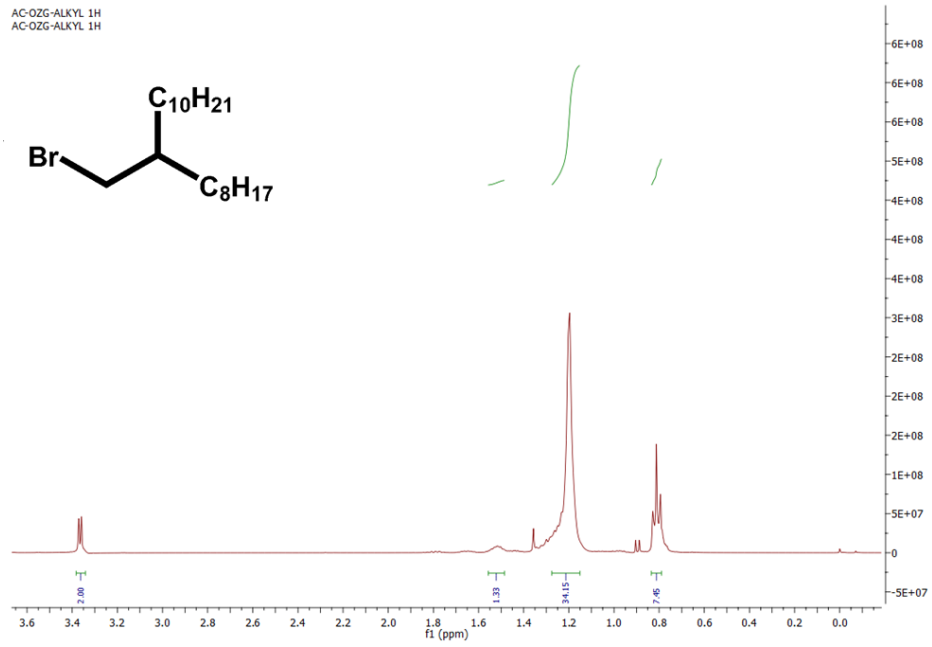

Figure 33. ^{1}H NMR of 9-(Bromomethyl)nonadecane

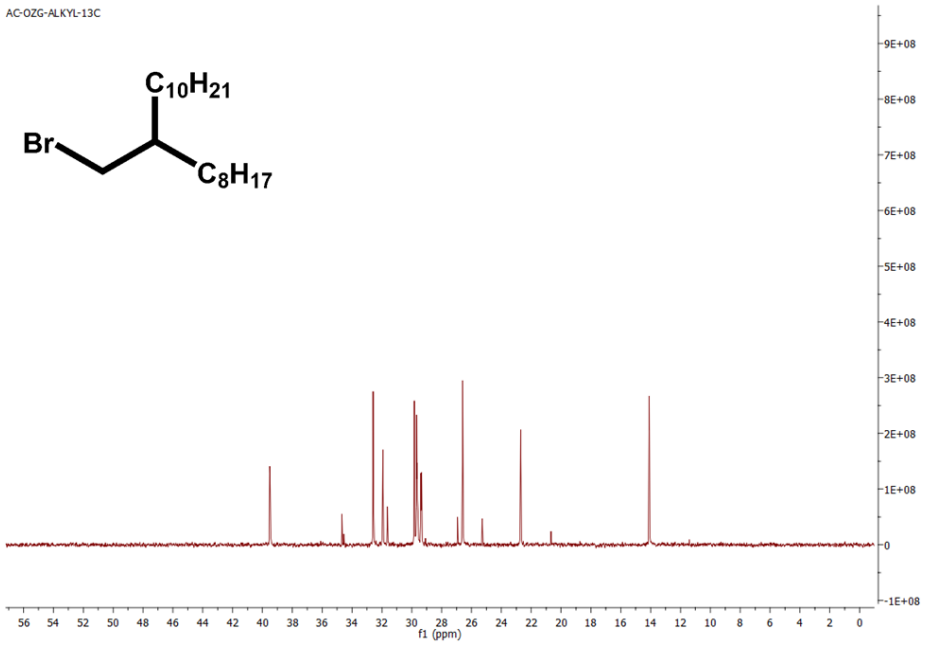

Figure 34. ^{13}C NMR of 9-(Bromomethyl)nonadecane

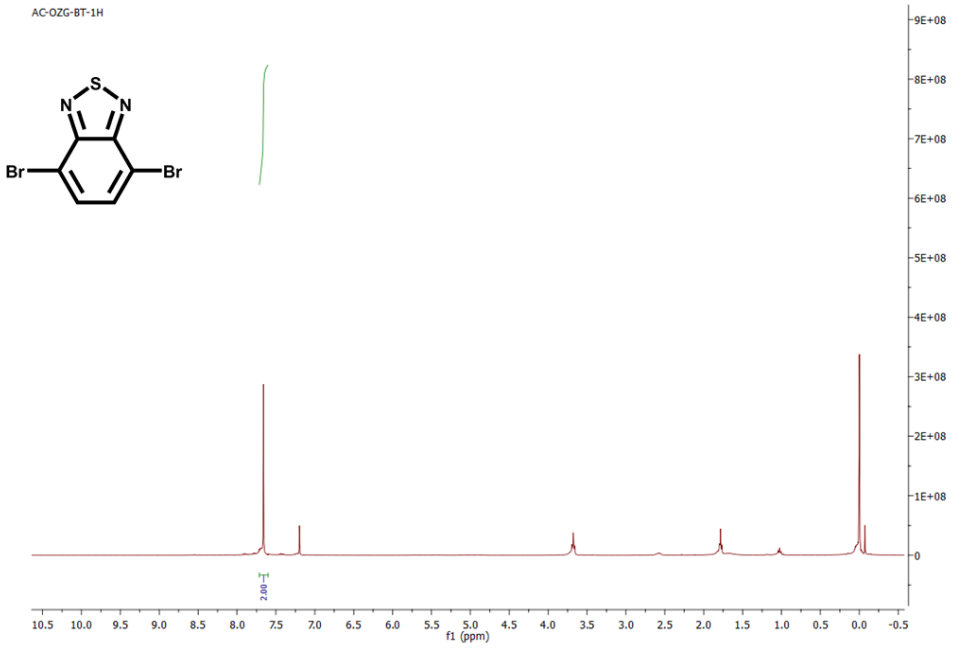

Figure 35. ^{1}H NMR of 4,7-Dibromobenzo[c][1,2,5]thiadiazole

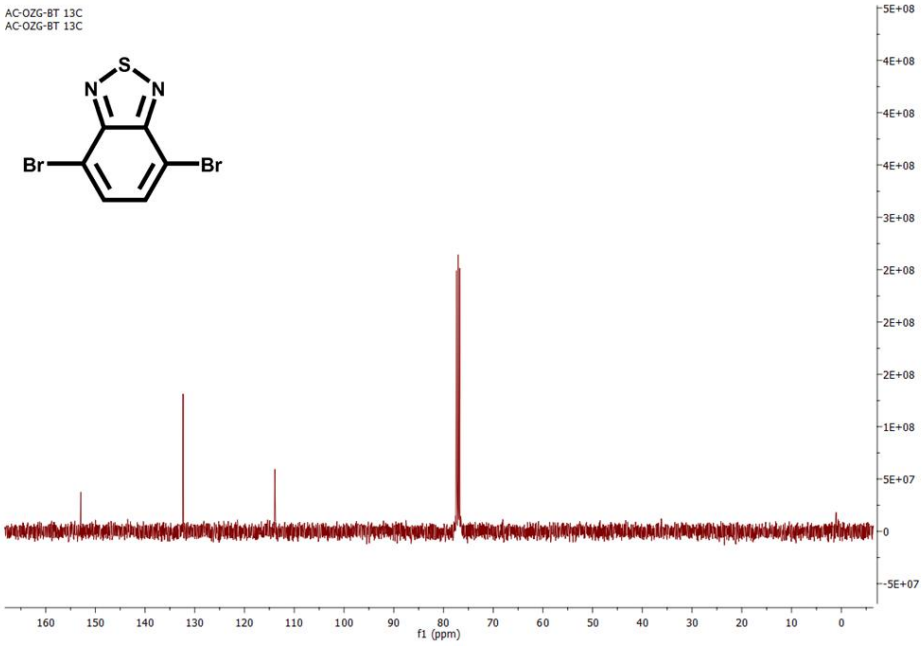

Figure 36. ^{13}C NMR of 4,7-Dibromobenzo[c][1,2,5]thiadiazole

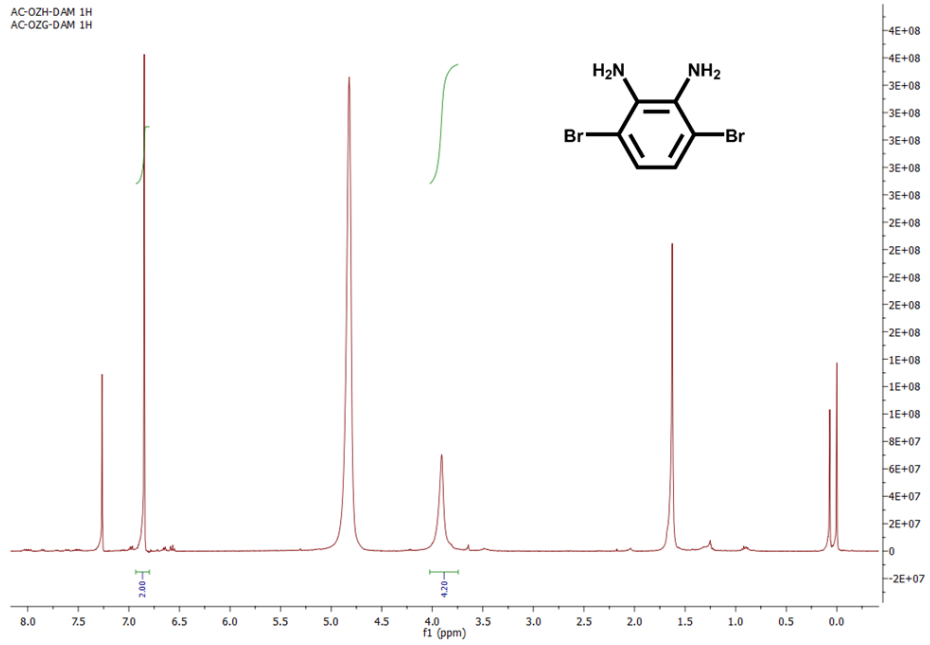

Figure 37. ^{1}H NMR of 3,6-Dibromobenzene-1,2-diamine

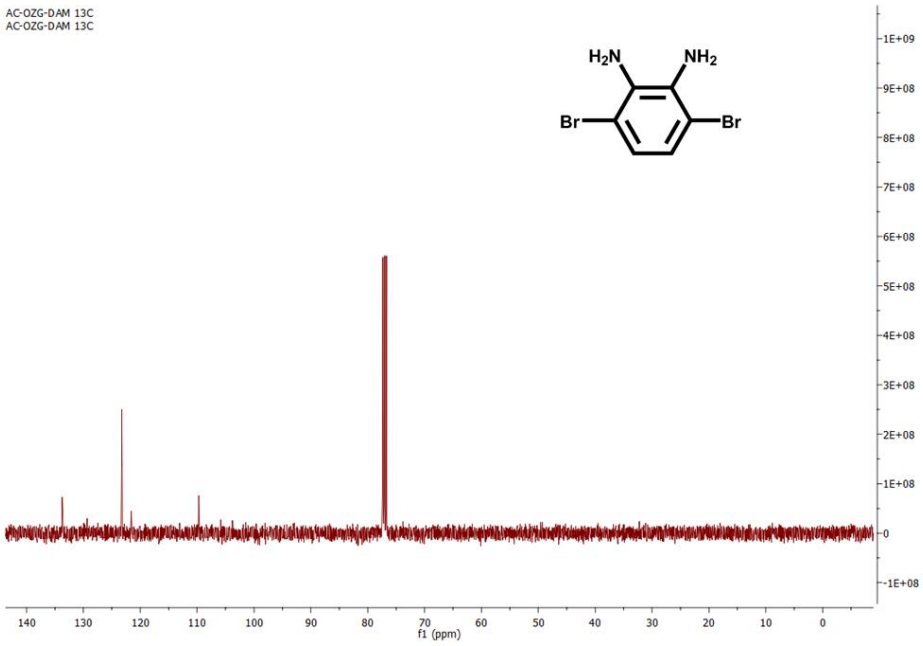

Figure 38. ^{13}C NMR of 4,7-Dibromobenzo[c][1,2,5]thiadiazole

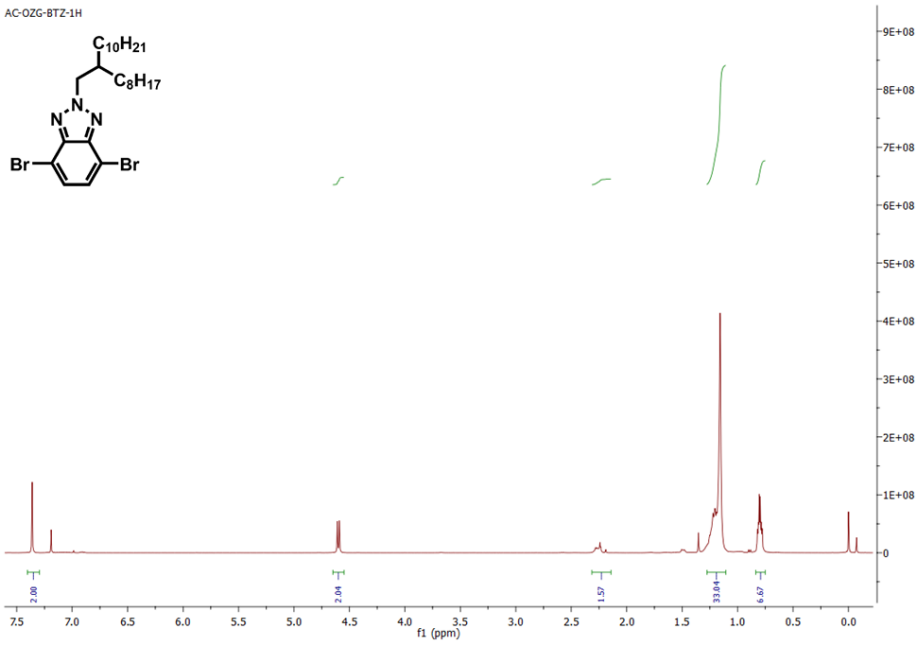

Figure 39. ^{1}H NMR of 4,7-Dibromo-2-(2-octyldodecyl)-2H-benzo[d][1,2,3]triazole

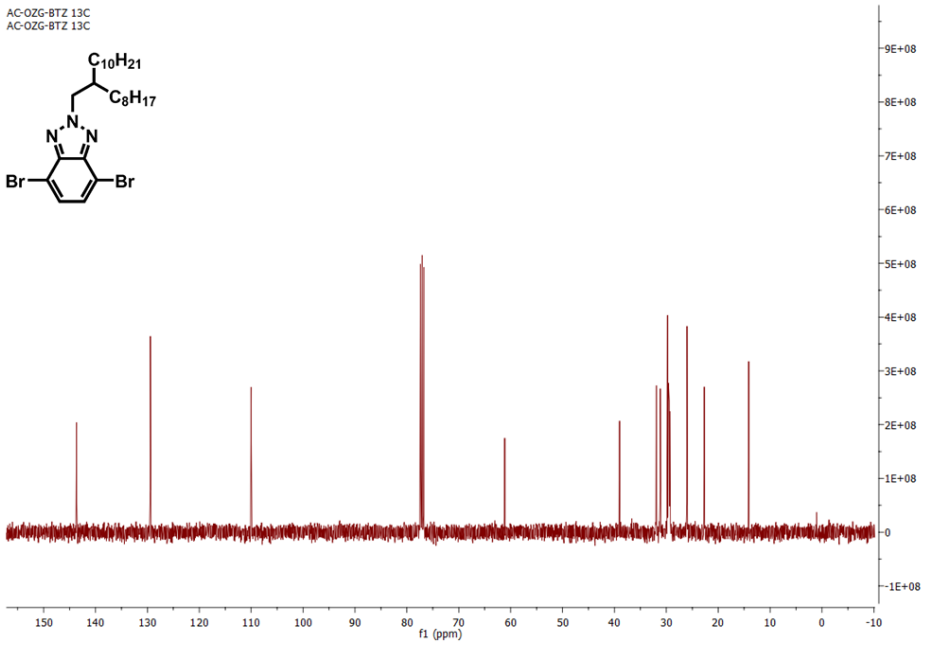

Figure 40. ^{13}C NMR of 7-Dibromo-2-(2-octyldodecyl)-2H-benzo[d][1,2,3]triazole

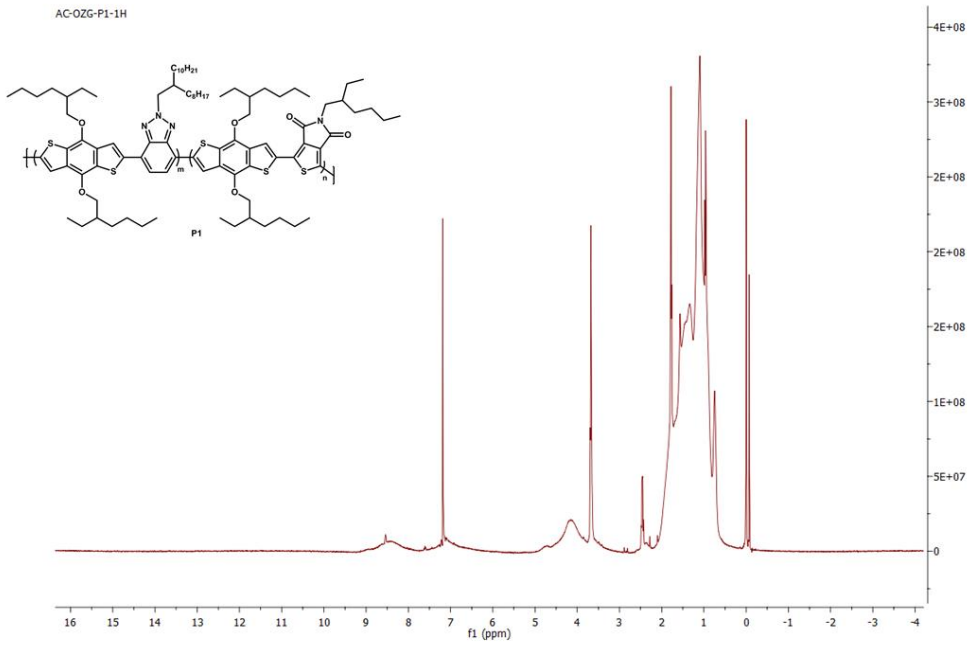

Figure 41. ^{1}H NMR of **P1**

THERMAL ANALYSIS RESULTS

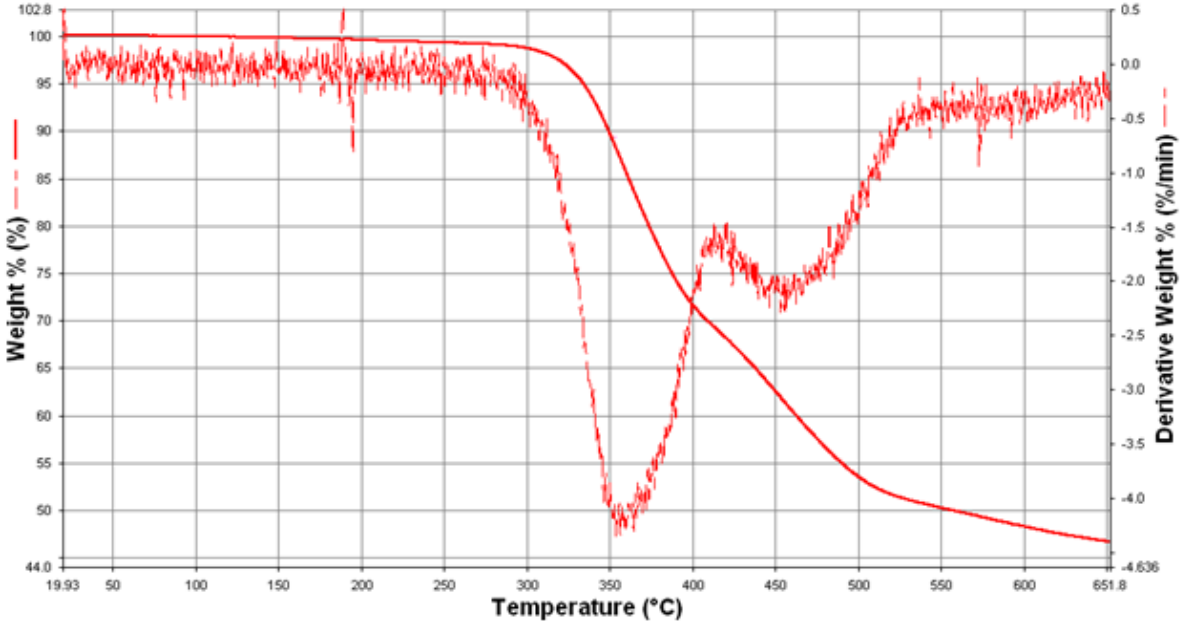

Figure 42. TGA Curve of **P1**

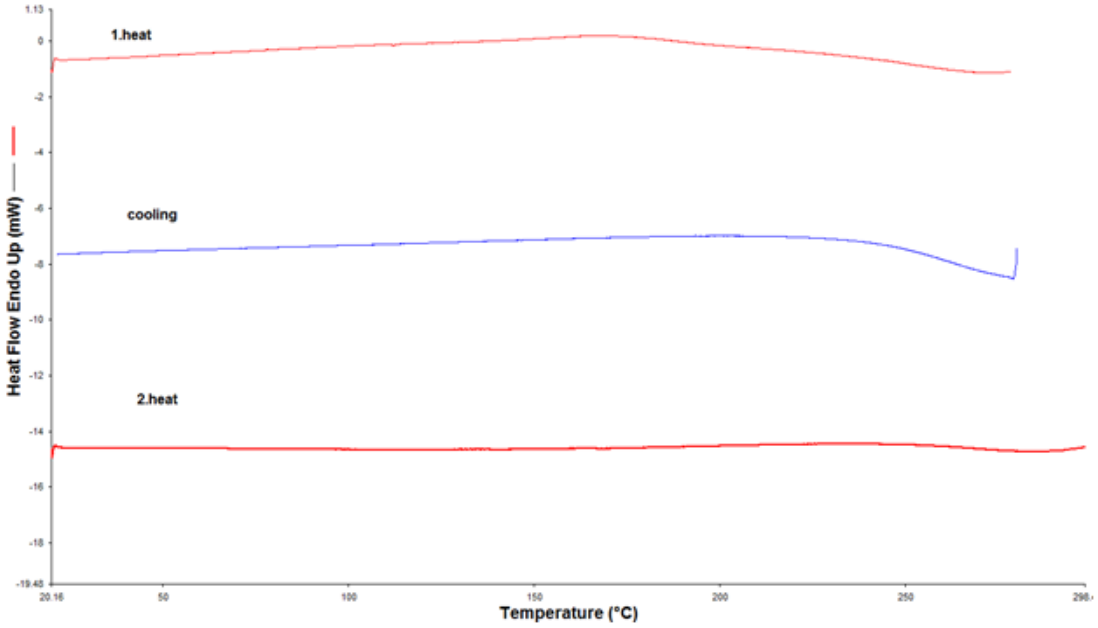

Figure 43. DSC Thermogram of **P1**

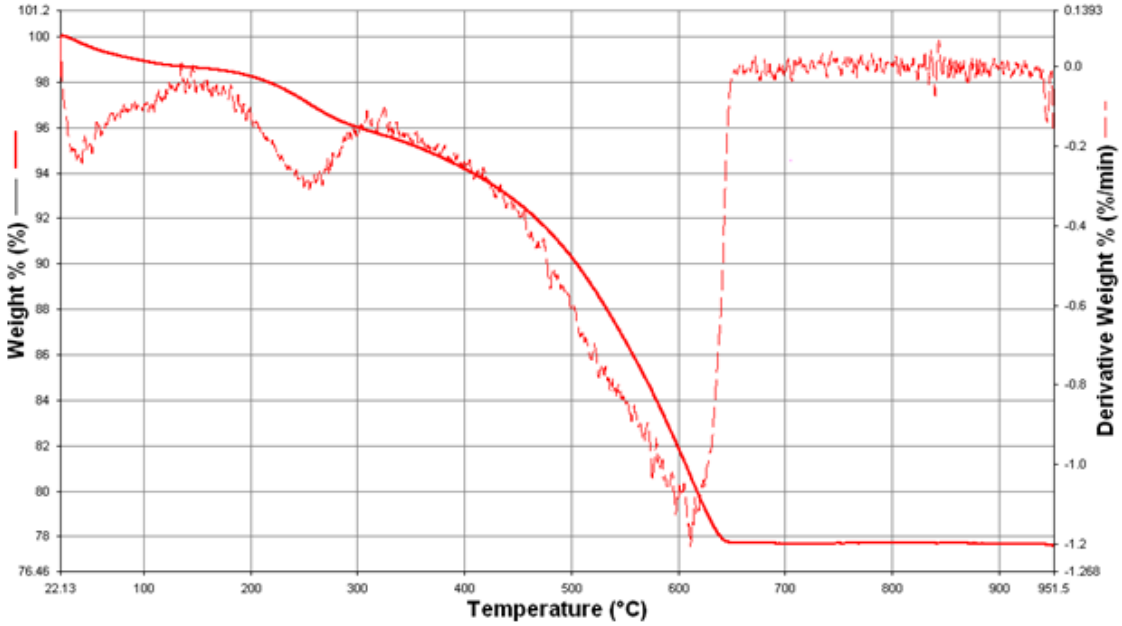

Figure 44. TGA Curve of **P2**

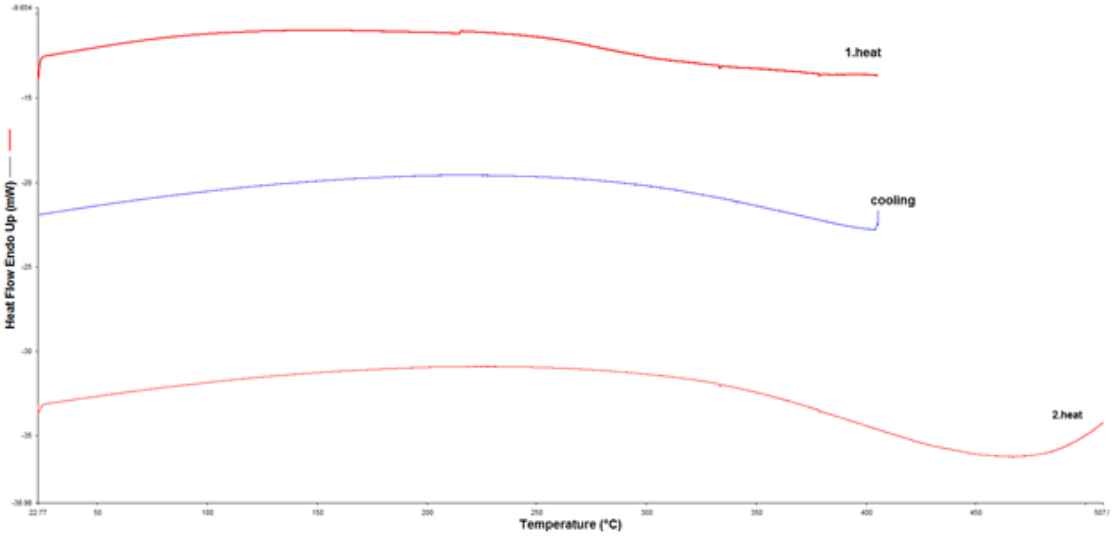

Figure 45. DSC Thermogram of **P2**